Axion Searches

P. Sikivie (IAS, UF)

Joint ILIAS-CAST-CERN Axion Training

C.E.R.N.

November 30, 2005

Outline

- Introduction
- Axion cosmology
- Dark matter axion detection
- Solar axion detection
- Laser experiments
- Other methods

The Strong CP Problem

$$L_{\mathrm{QCD}} = \;\ldots + \;\theta \frac{g^2}{32\pi^2} G^a{}_{\mu\nu}\, \tilde{G}^{a\mu\nu}$$

Because the strong interactions conserve P and CP, $\theta \leq 10^{-10}$.

The Standard Model does not provide a reason for θ to be so tiny,

but a relatively small modification of the model does provide a reason …

If a $\mathrm{U_{PQ}(1)}$ symmetry is assumed,

$$L = \ldots + \frac{a}{f_a}\frac{g^2}{32\pi^2} G^a{}_{\mu\nu}\tilde{G}^{a\mu\nu} + \frac{1}{2}\partial_\mu a\, \partial^\mu a + \ldots$$

$\theta = \dfrac{a}{f_a}$ relaxes to zero,

and a light neutral pseudoscalar particle is predicted: the axion.

$$m_a \simeq 6 \text{ eV} \; \frac{10^6 \text{ GeV}}{f_a}$$

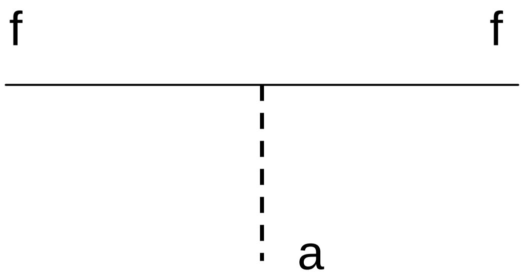

$$L_{a\bar{f}f} = i\, g_f \,\frac{a}{f_a}\; \bar{f}\, \gamma_5\, f$$

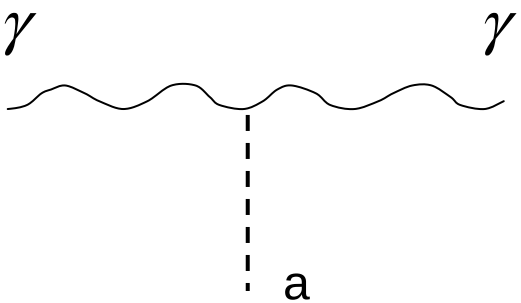

$$L_{a\gamma\gamma} = g_\gamma \,\frac{\alpha}{\pi}\, \frac{a}{f_a}\, \vec{E}\cdot\vec{B}$$

g_γ = 0.97 in KSVZ model
0.36 in DFSZ model

The remaining axion window

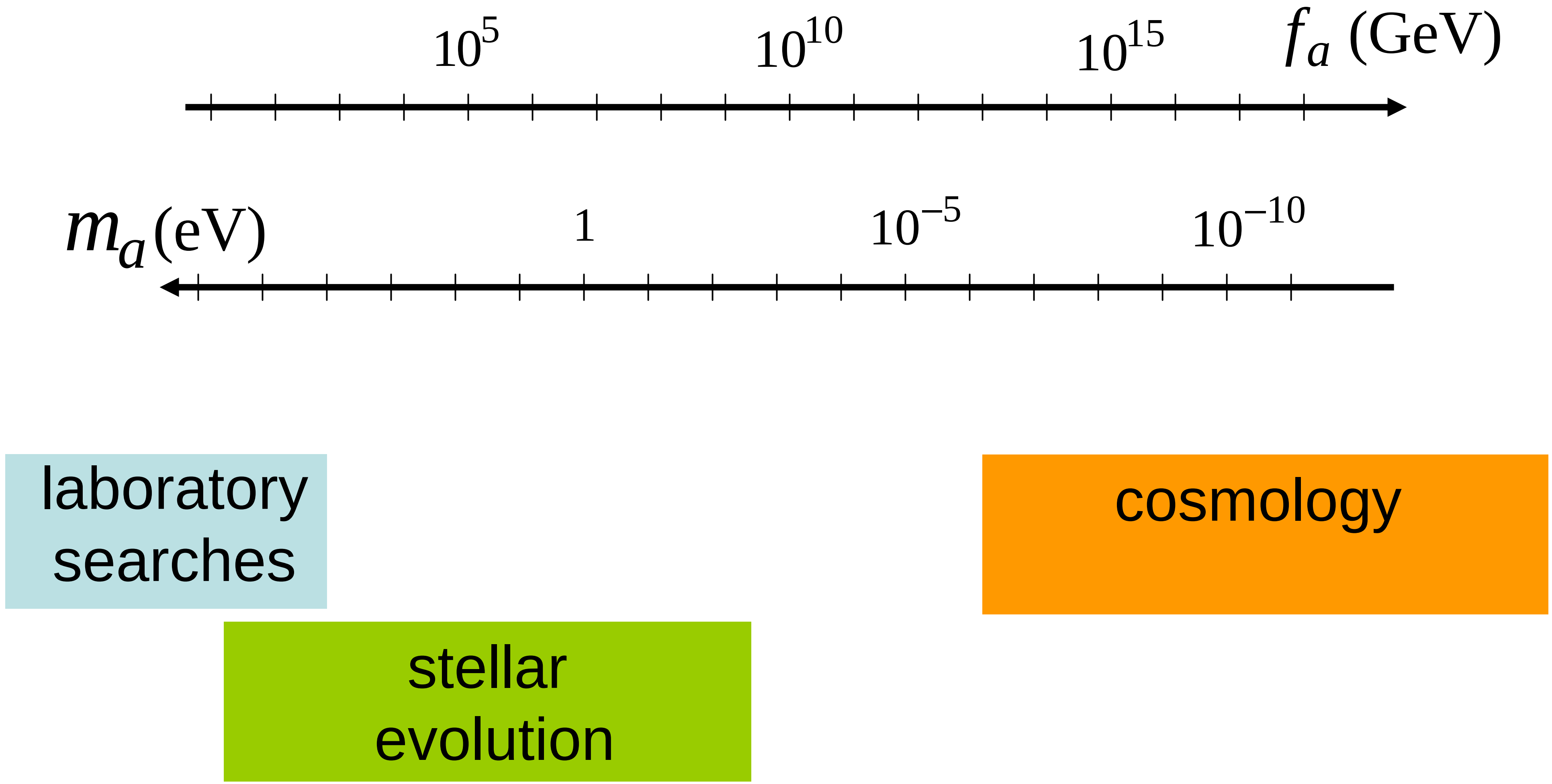

There are two cosmic axion populations: hot and cold.

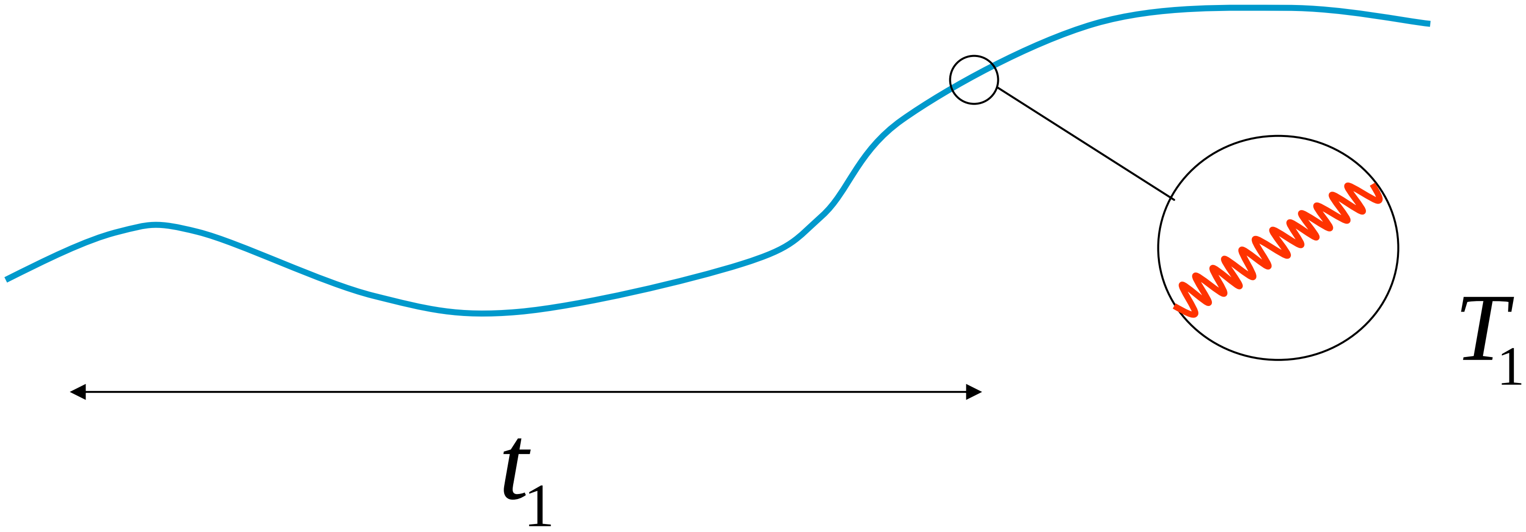

When the axion mass turns on, at QCD time,

$$t_1 \sim 2 \cdot 10^{-7}\ \text{sec}$$

$$T_1 \sim 1\ \text{GeV}$$

$$p_a(t_1) = \frac{1}{t_1} \sim 3 \cdot 10^{-9}\ \text{eV}$$

Thermal axions

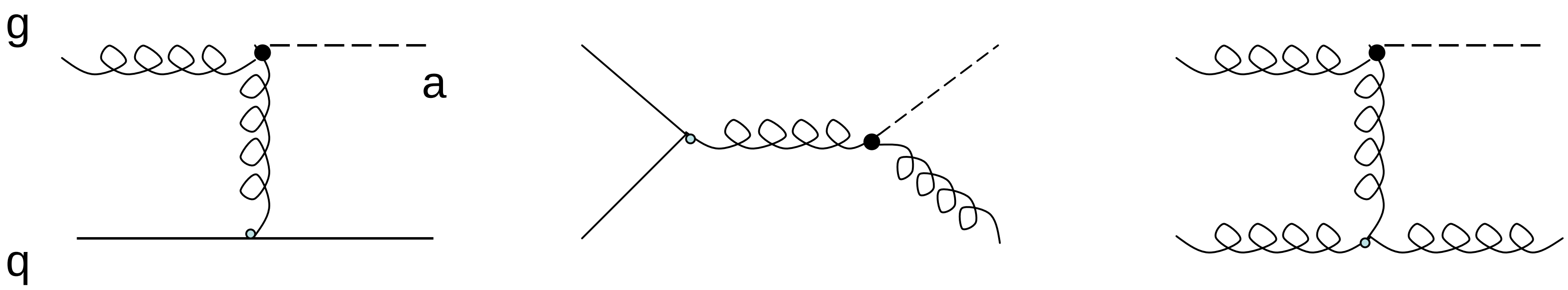

these processes imply an axion decoupling temperature

$$T_D \simeq 3 \cdot 10^{11}\ \mathrm{GeV} \left(\frac{f_a}{10^{12}\ \mathrm{GeV}} \right)^2$$

E. Masso
R. Rota
G. Zsembinszki

thermal axion
temperature today:

$$T_a\,(t_0) = 0.908\ \mathrm{K} \left(\frac{106.75}{N_D} \right)^{\frac{1}{3}}$$

N_D = effective number of thermal degrees of freedom at axion decoupling

Cold Axions

Density $$\Omega_a \approx \left(\frac{10^{-5}\ \mathrm{eV}}{m_a} \right)^{\frac{7}{6}}$$

Velocity dispersion

$$\delta \mathrm{v}_a (t_0) \sim 3 \cdot 10^{-17}\, c \left(\frac{10^{-5}\ \mathrm{eV}}{m_a} \right)^{\frac{5}{6}}$$

Effective temperature

$$T_{a,\,\mathrm{eff}} (t_0) \sim 10^{-34}\ \mathrm{K} \left(\frac{10^{-5}\ \mathrm{eV}}{m_a} \right)^{\frac{2}{3}}$$

Effective potential V(T,Φ)

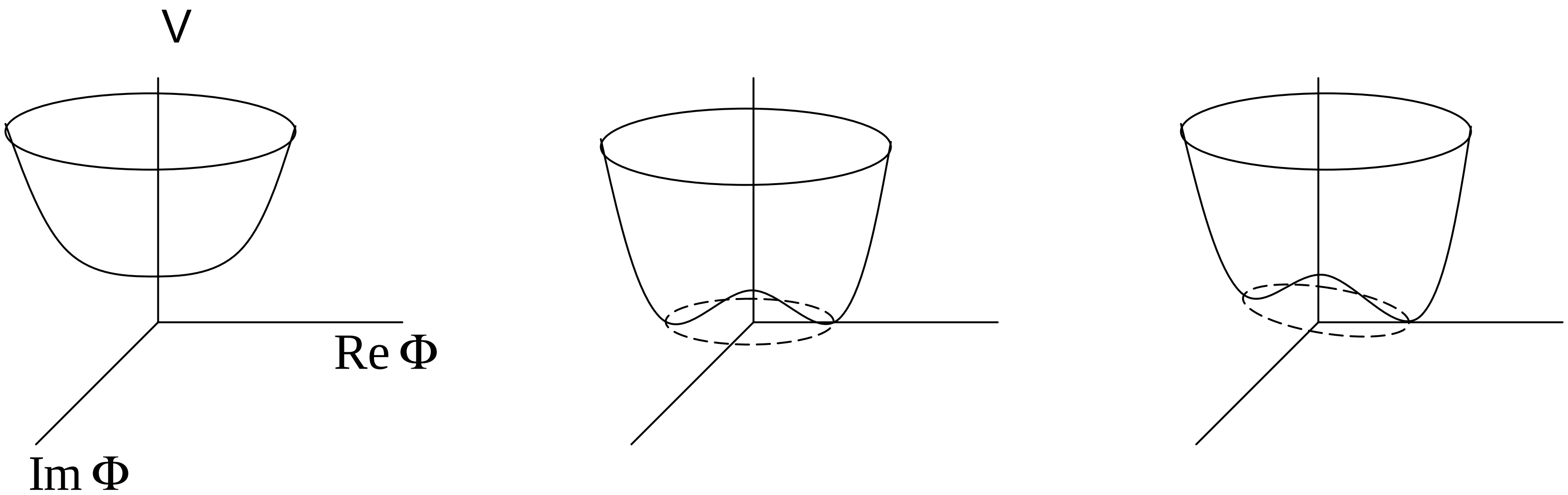

$T > f_a$

$f_a > T > 1\,\mathrm{GeV}$

↓

axion strings

$1\,\mathrm{GeV} > T$

↓

axion domain walls

Axion production by vacuum realignment

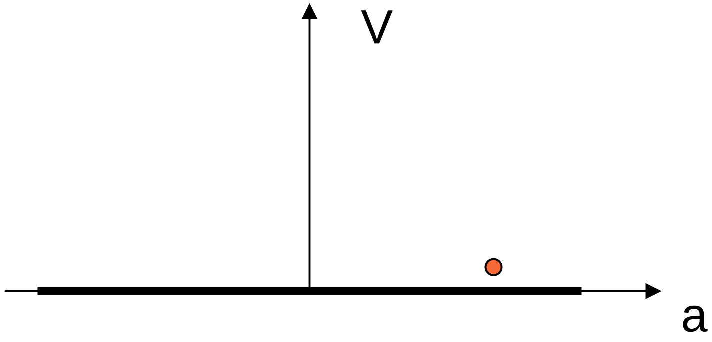

$T \geq 1\,\mathrm{GeV}$

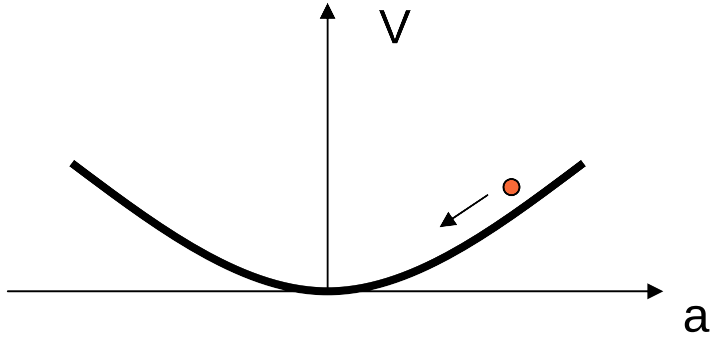

$T \leq 1\,\mathrm{GeV}$

$$n_a(t_1) \sim \frac{1}{2} m_a(t_1)\, a(t_1)^2 \sim \frac{1}{2t_1} f_a^{\,2}\, \alpha(t_1)^2$$

initial misalignment angle

$$\rho_a(t_0) \sim m_a\, n_a(t_1) \left(\frac{R_1}{R_0}\right)^3 \propto m_a^{-\frac{7}{6}}$$

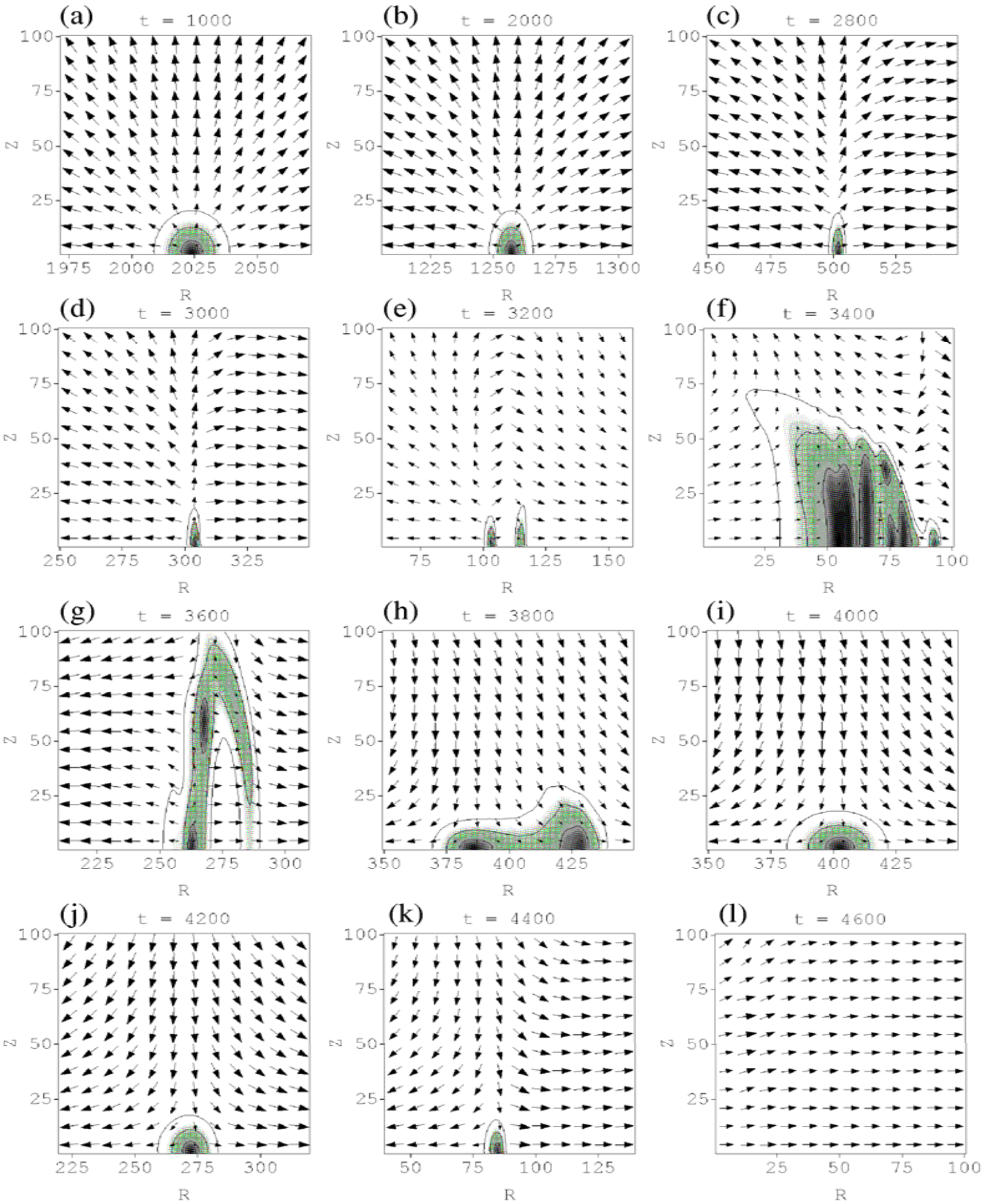

String loop decaying into axion radiation

simulation by
S. Chang, C. Hagmann and PS

see also:
R. Battye and P. Shellard;

M. Yamaguchi, M.Kawasaki and J. Yokoyama

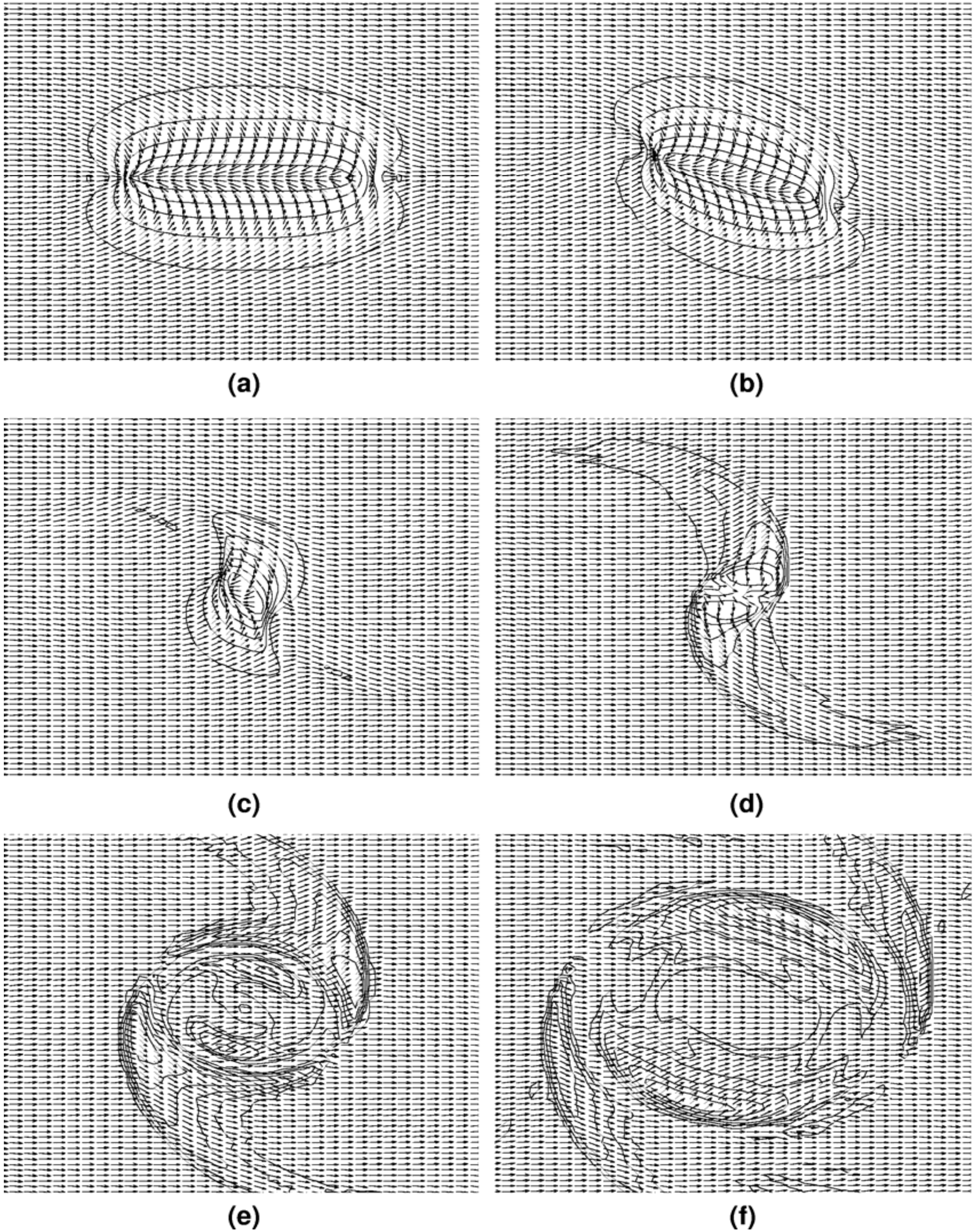

Domain wall bounded by string decaying into axion radiation

If inflation after the PQ phase transition

- $$\Omega_a \sim 0.25 \left(\frac{10^{-5}\ \mathrm{eV}}{m_a} \right)^{\frac{7}{6}} \alpha(t_1)^2$$ may be accidentally suppressed

- $$< \sqrt{a^2} > \sim \frac{H_I}{2\pi}$$ produces isocurvature density perturbations

$$\left.\frac{\delta\rho_a}{\rho_a}\right|_{\substack{\text{iso}\\ \text{curvature}}} \sim \frac{H_I}{f_a\, \alpha(t_1)} \leq 10^{-6}$$

CMBR constraint

If no inflation after the PQ phase transition

- cold axions are produced by vacuum realignment, string decay and wall decay

$$\Omega_a \sim 0.5 \left(\frac{10^{-5}\ \text{eV}}{m_a} \right)^{\frac{7}{6}}$$

- axion miniclusters appear

(Hogan and Rees, Kolb and Tkachev)

$$M_{\text{mc}} \sim 10^{-13}\, M_{\odot} \left(\frac{10^{-5}\ \text{eV}}{m_a} \right)^{\frac{5}{3}} \qquad l_{\text{mc}} \sim 10^{13}\ \text{cm} \left(\frac{10^{-5}\ \text{eV}}{m_a} \right)^{\frac{1}{6}}$$

D.B. Kaplan and K.M. Zurek (hep-ph/0507236)

introduce $f_a(t)$

require $f_a(t_0) > 10^9\ \mathrm{GeV}$ for stellar evolution

$$\rho_a(t_0) \propto m_a(t_0)\, n_a(t_1)\left(\frac{R_1}{R_0}\right)^3 \propto \frac{1}{f_a(t_0)}\, f_a^{\,2}(t_1)$$

arrange $f_a(t_1) \ll f_a(t_0)$ for cosmological energy density

allows $f_a(t_0)$ much larger than 10^{12} GeV

Axion dark matter is detectable

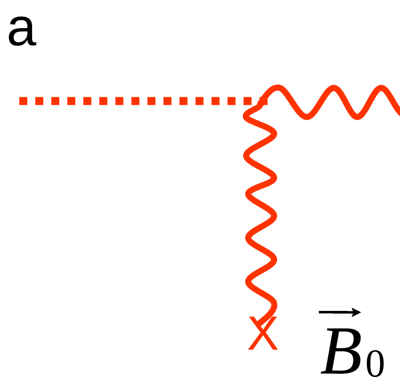

$$L_{a\gamma\gamma} = g_\gamma \frac{\alpha}{\pi} \frac{a}{f_a} \vec{E} \cdot \vec{B}$$

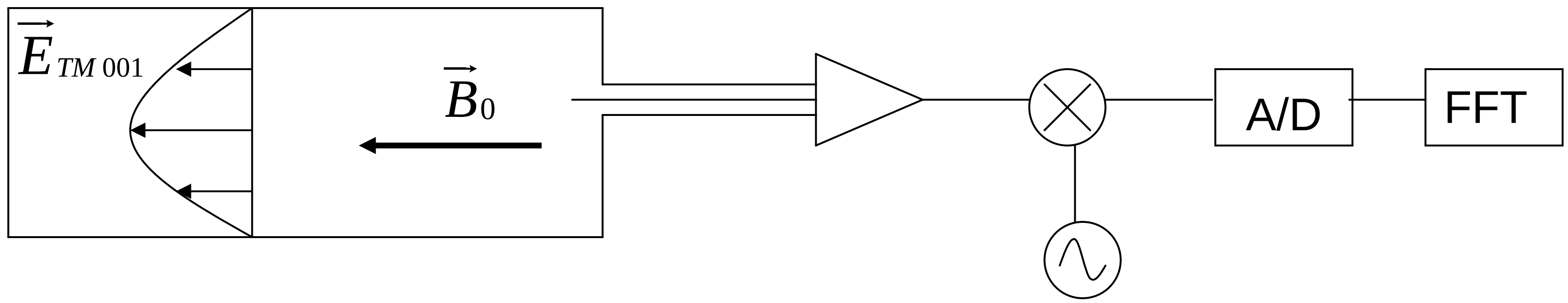

$$h\nu = m_a c^2 \left(1 + \frac{1}{2}\beta^2\right)$$

$$\beta = \frac{v}{c} \,\square\, 10^{-3}$$

$$Q_a \,\square\, 10^{-6}$$

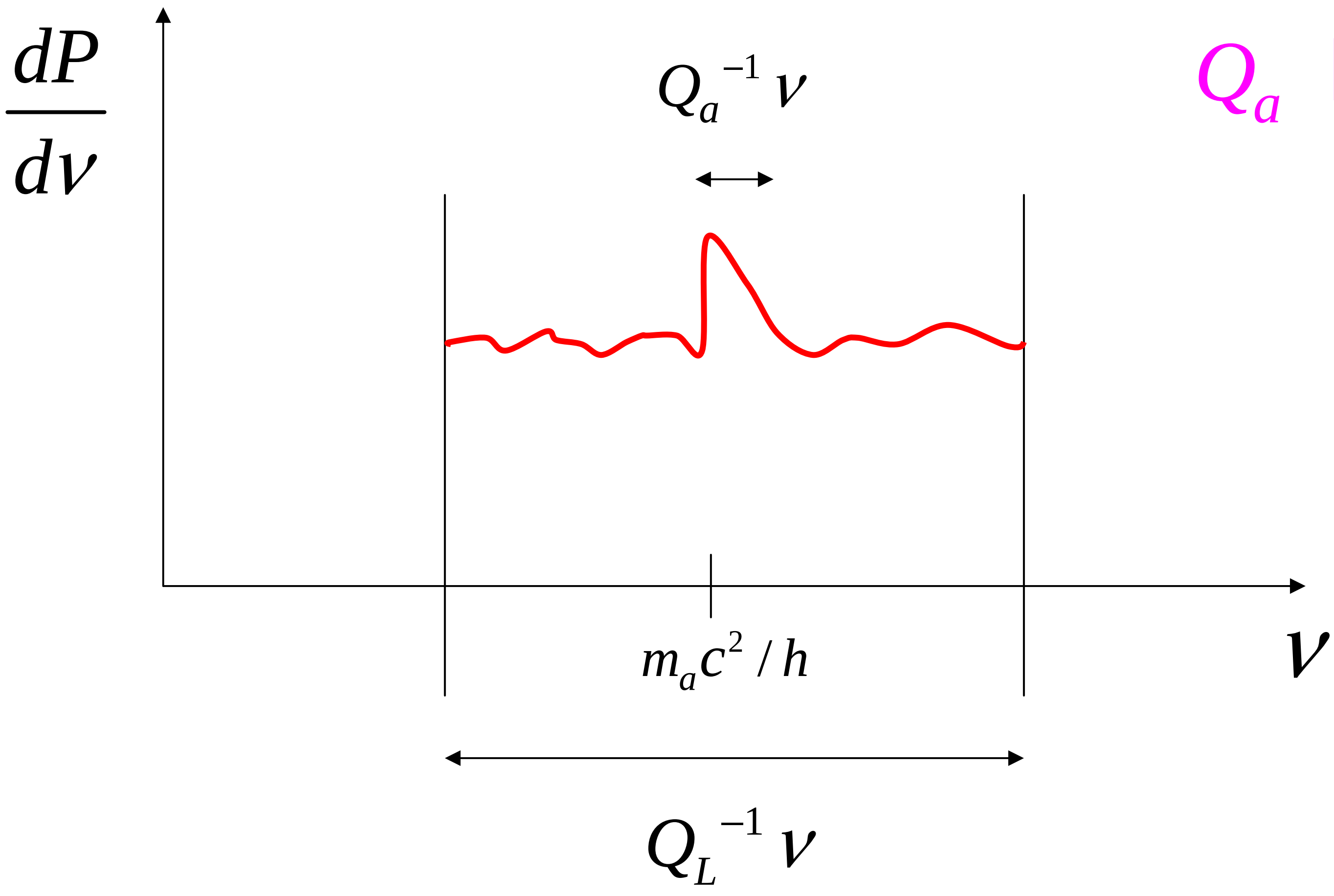

$a \to \gamma$

conversion power on resonance

$$P = \left(\frac{\alpha g_\gamma}{\pi f_a}\right)^2 V\, B_0^{\,2}\, \rho_a\, C\, m_a^{\,-1}\, Q_L$$

$$= \; 2\cdot 10^{-22}\ \text{Watt}\left(\frac{V}{500\ \text{liter}}\right)\left(\frac{B_0}{7\ \text{Tesla}}\right)^2\left(\frac{C}{0.4}\right)$$

$$\left(\frac{g_\gamma}{0.36}\right)^2\left(\frac{\rho_a}{5\cdot 10^{-25}\ \text{gr/cm}^3}\right)\left(\frac{m_a c^2}{h\ \text{GHz}}\right)\left(\frac{Q_L}{10^5}\right)$$

search rate for s/n = 4

$$\frac{df}{dt} = \frac{1.2\ \text{GHz}}{\text{year}}\left(\frac{P}{2\cdot 10^{-22}\ \text{Watt}}\right)^2\left(\frac{3\,K}{T_n}\right)^2$$

Axion Dark Matter eXperiment

Magnet with Insert (side view)

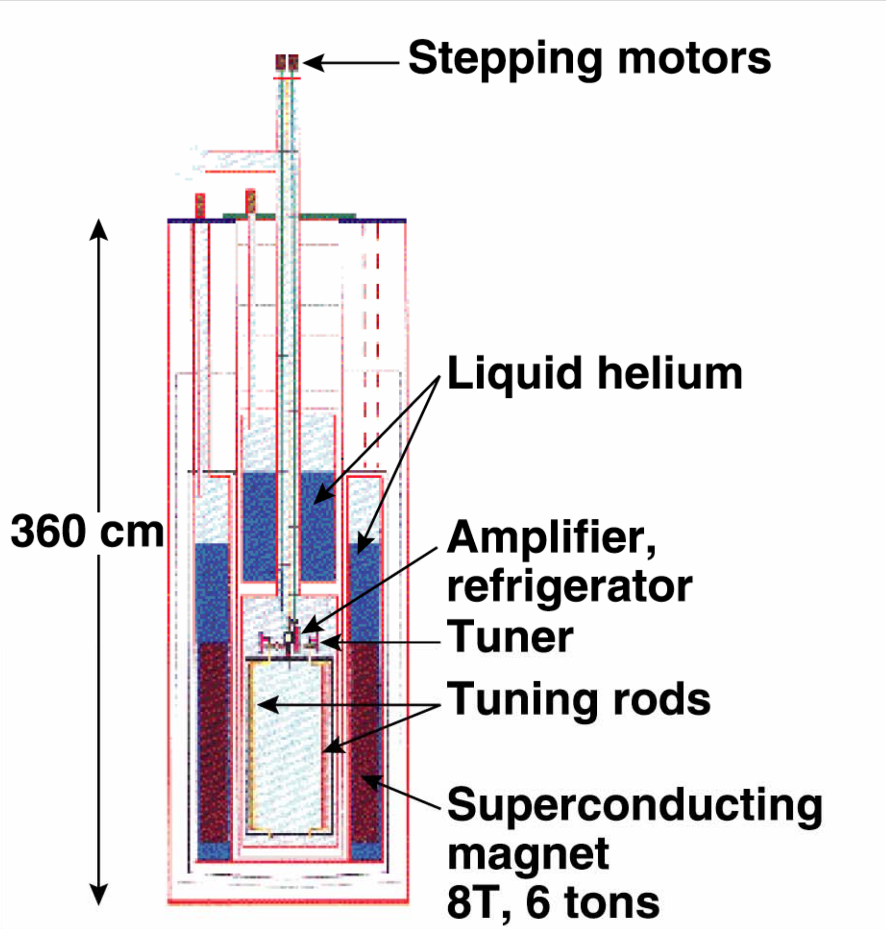

Pumped LHe → T ~ 1.5 k

Magnet

8 T, 1 m × 60 cm ∅

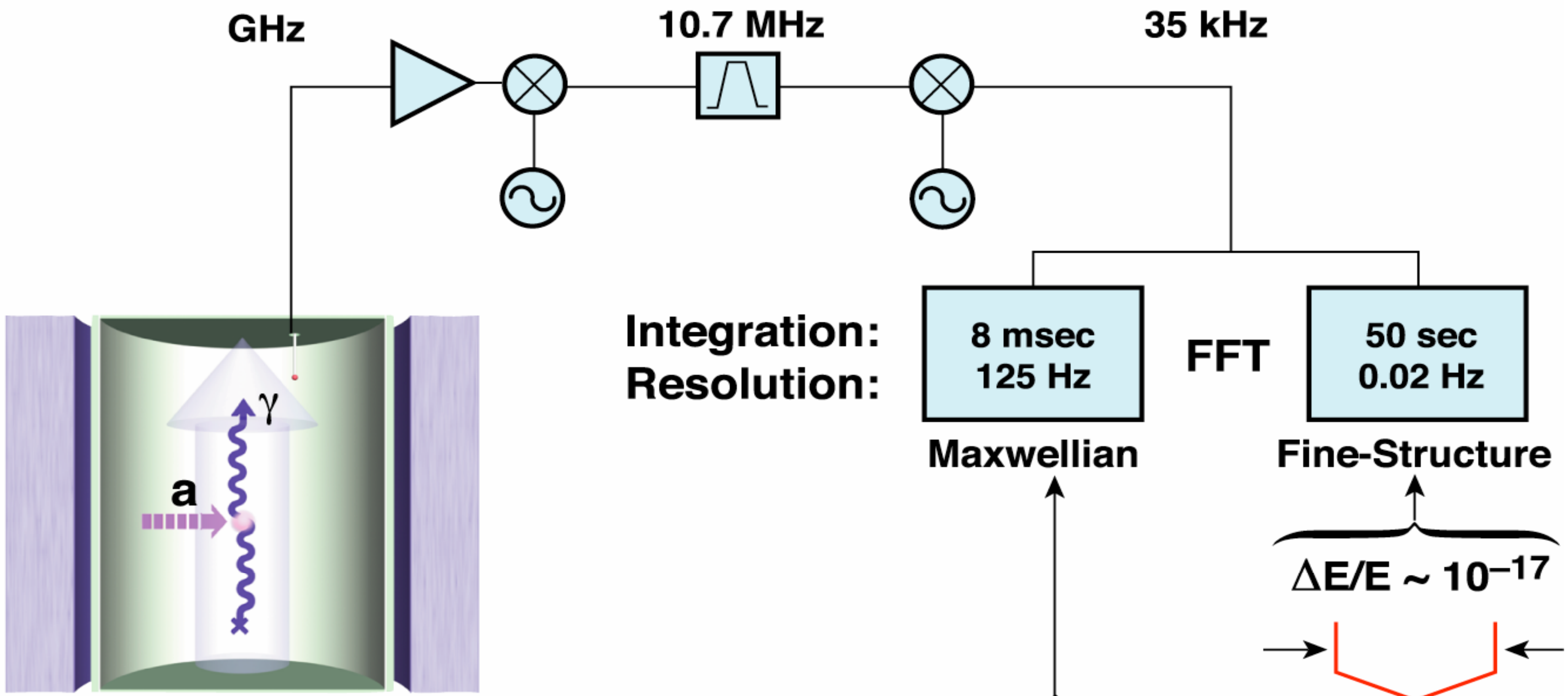

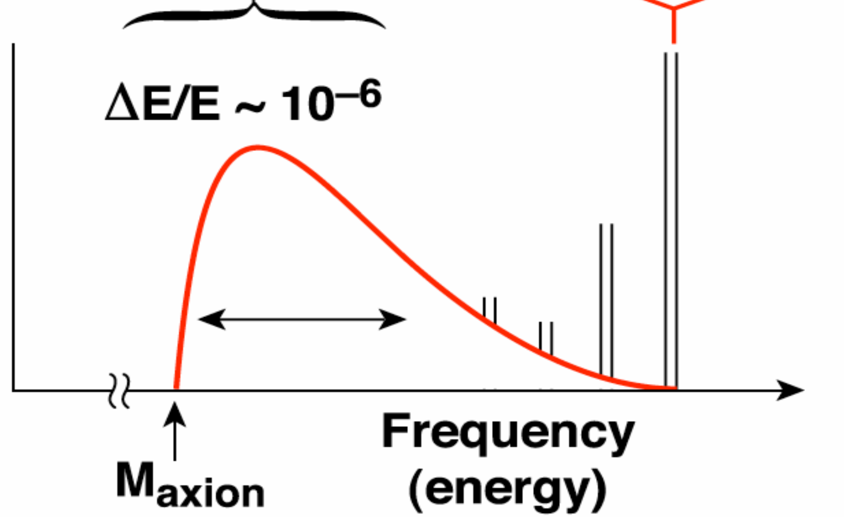

High resolution analysis of the signal may reveal fine structure …

The cold dark matter particles lie on a 3-dimensional sheet in 6-dimensional phase space

the physical density is the projection of the phase space sheet onto position space

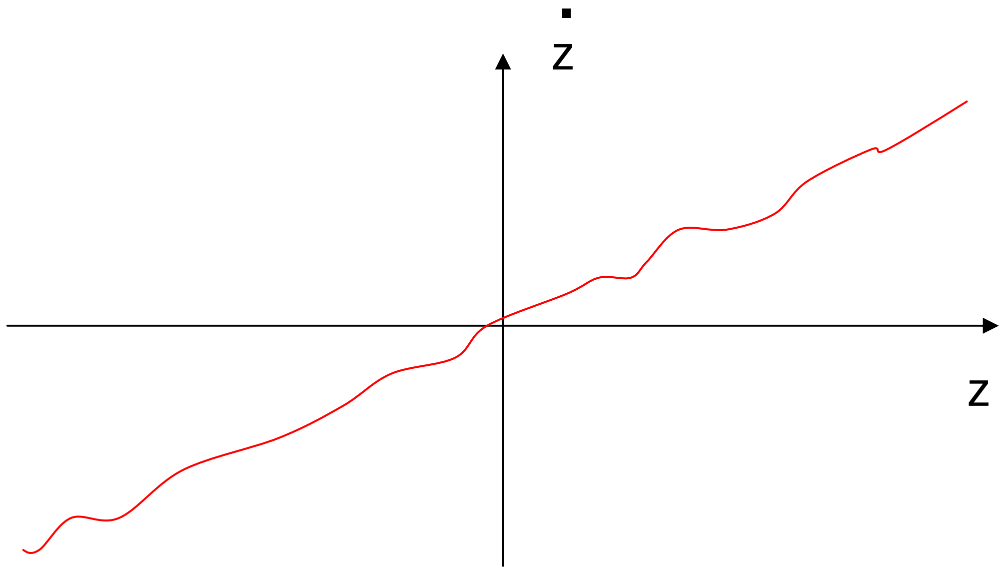

$$\vec{v}(\vec{r},t) = H(t)\,\vec{r} + \Delta\vec{v}(\vec{r},t)$$

The cold dark matter particles lie on a 3-dimensional sheet in 6-dimensional phase space

the physical density is the projection of the phase space sheet onto position space

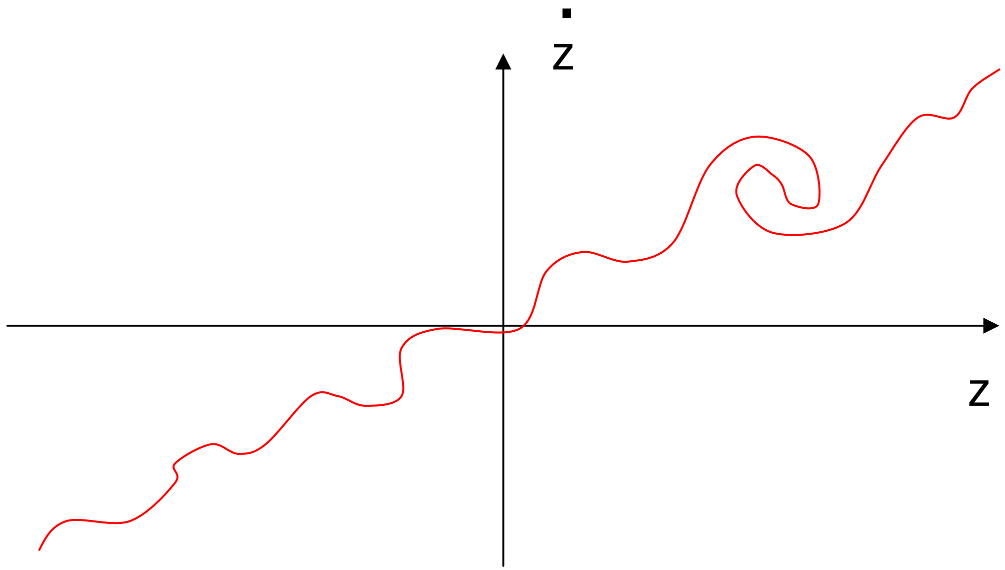

$$\vec{v}(\vec{r},t) = H(t)\,\vec{r} + \Delta\vec{v}(\vec{r},t)$$

Implications:

1. At every point in physical space, the distribution of velocities is discrete, each velocity corresponding to a particular flow at that location.

2. At some locations in physical space, where the number of flows changes, there is a caustic, i.e. the density of dark matter is very high there.

Phase space structure of spherically symmetric halos

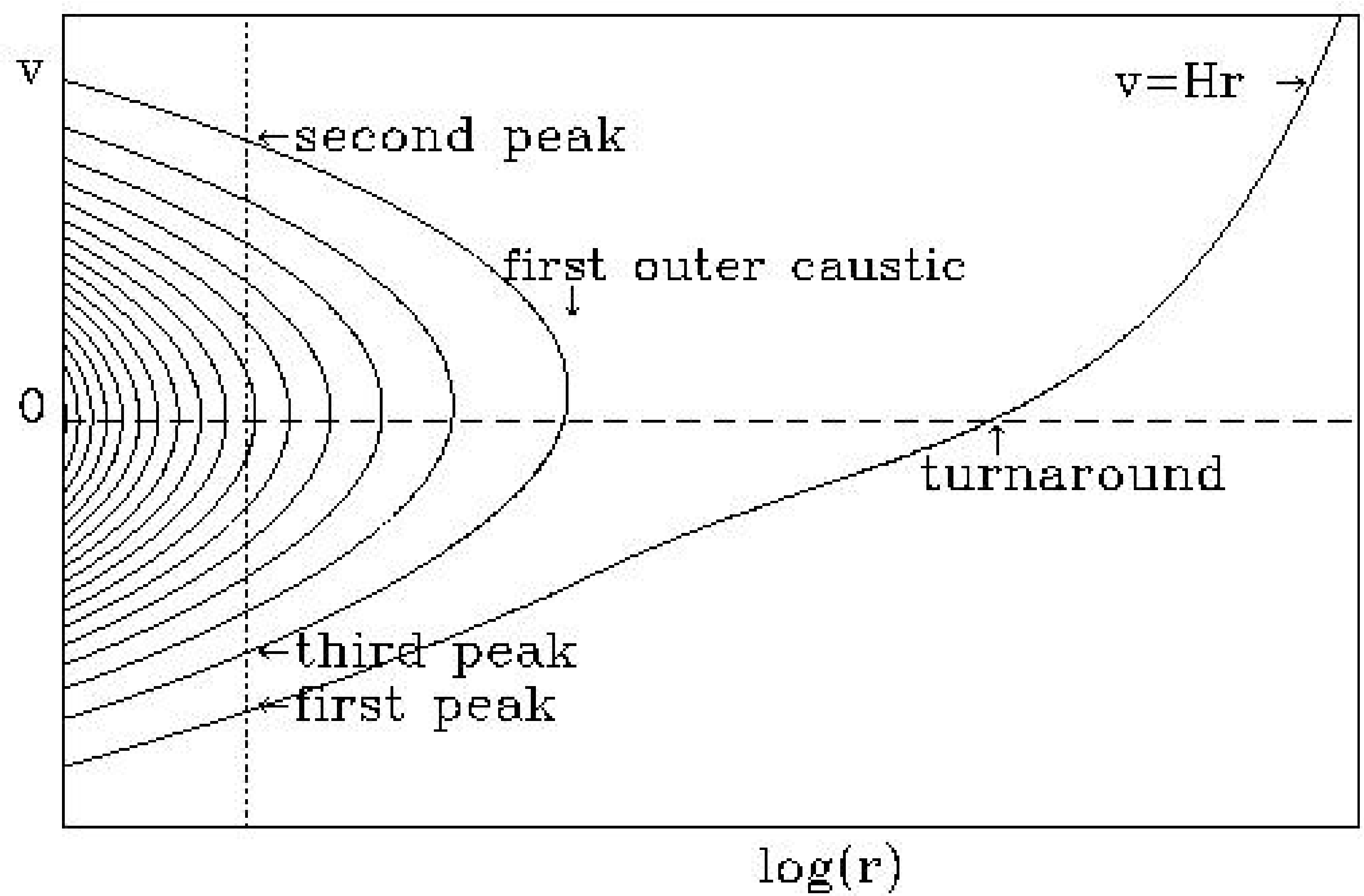

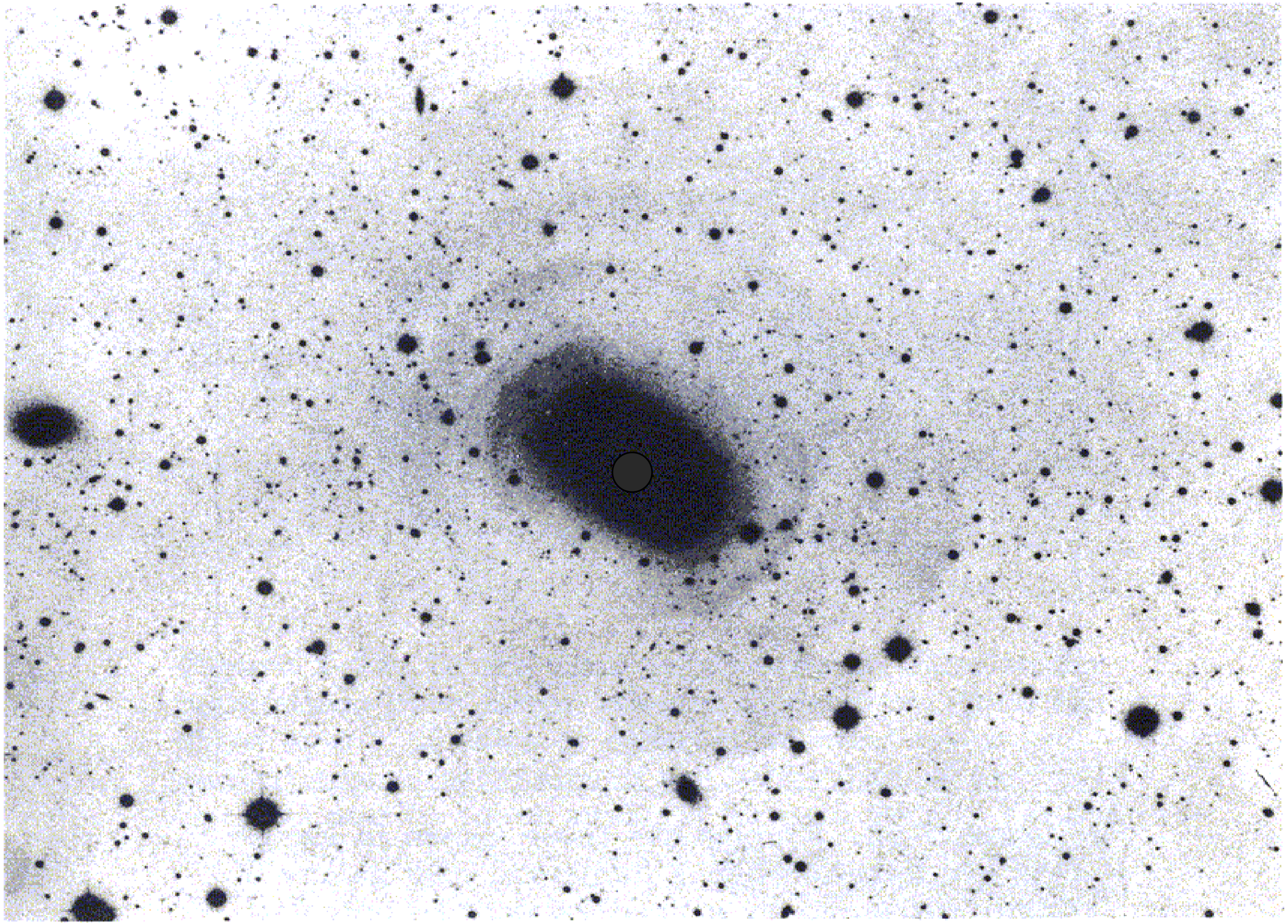

Figure 7-22. The giant elliptical galaxy NGC 3923 is surrounded by faint ripples of brightness. Courtesy of D. F. Malin and the Anglo-Australian Telescope Board.

(from Binney and Tremaine's book)

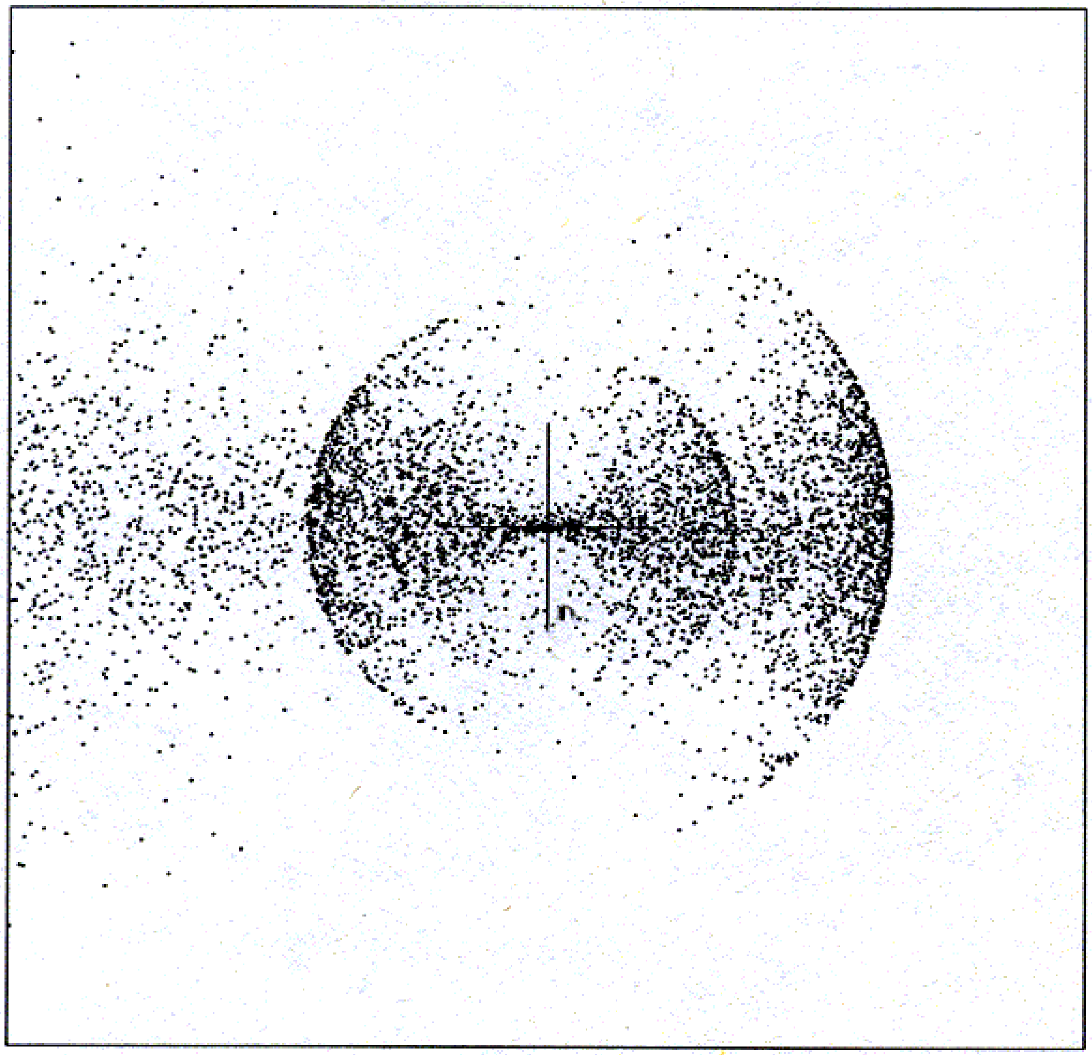

Figure 7-23. Ripples like those shown in Figure 7-22 are formed when a numerical disk galaxy is tidally disrupted by a fixed galaxy-like potential. (See Hernquist & Quinn 1987.)

The flow of cold collisionless particles from all directions in and out of a region necessarily forms a caustic (Arvind Natarajan and PS, astro-ph/0510743).

Hence galactic halos have inner caustics as well as outer caustics.

If the initial velocity field is dominated by net overall rotation, the inner caustic is a ‘tricusp ring’.

If the initial velocity field is irrotational, the inner caustic has a ‘tent-like’ structure.

simulation by Arvind Natarajan

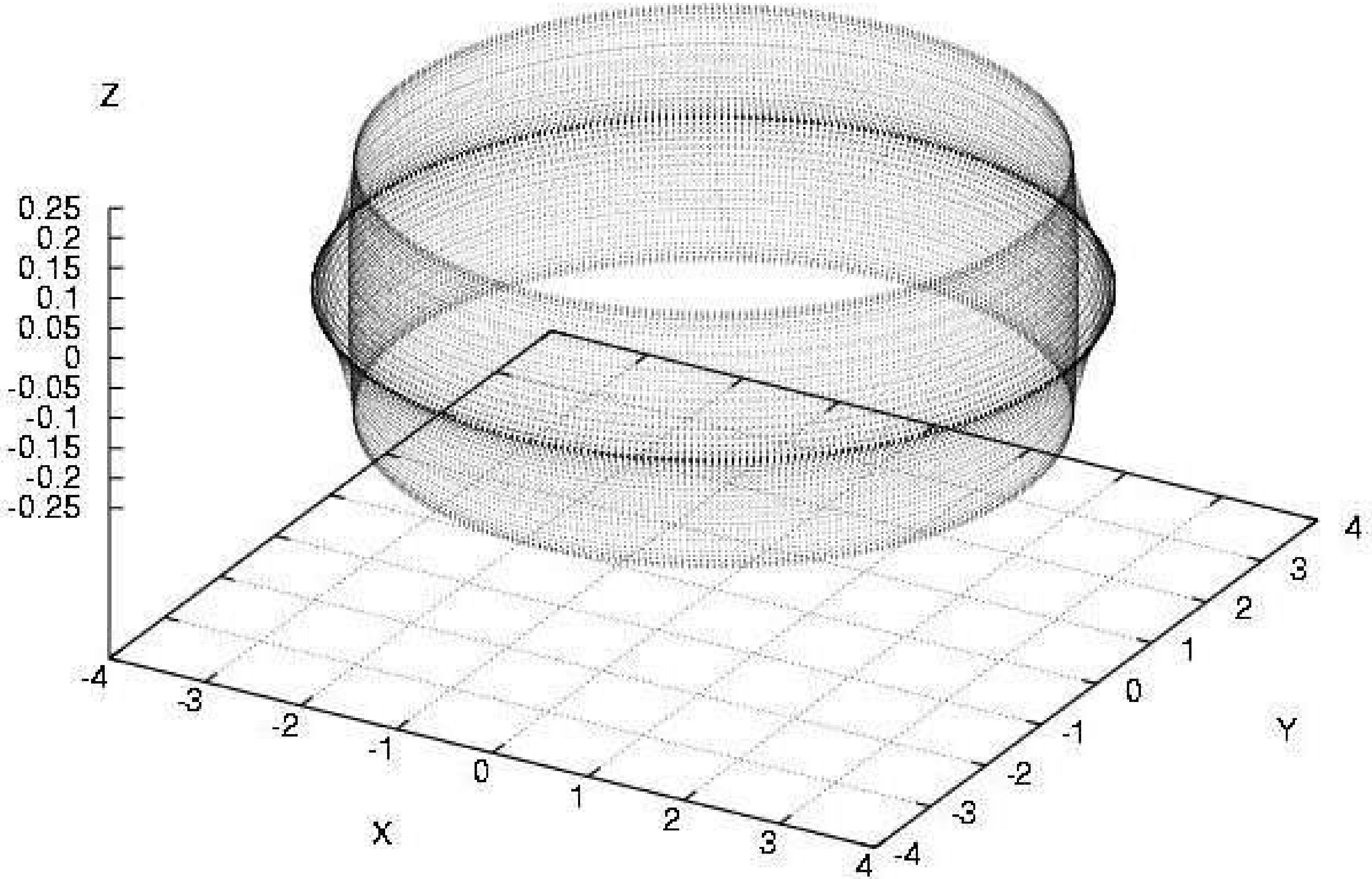

The caustic ring cross-section

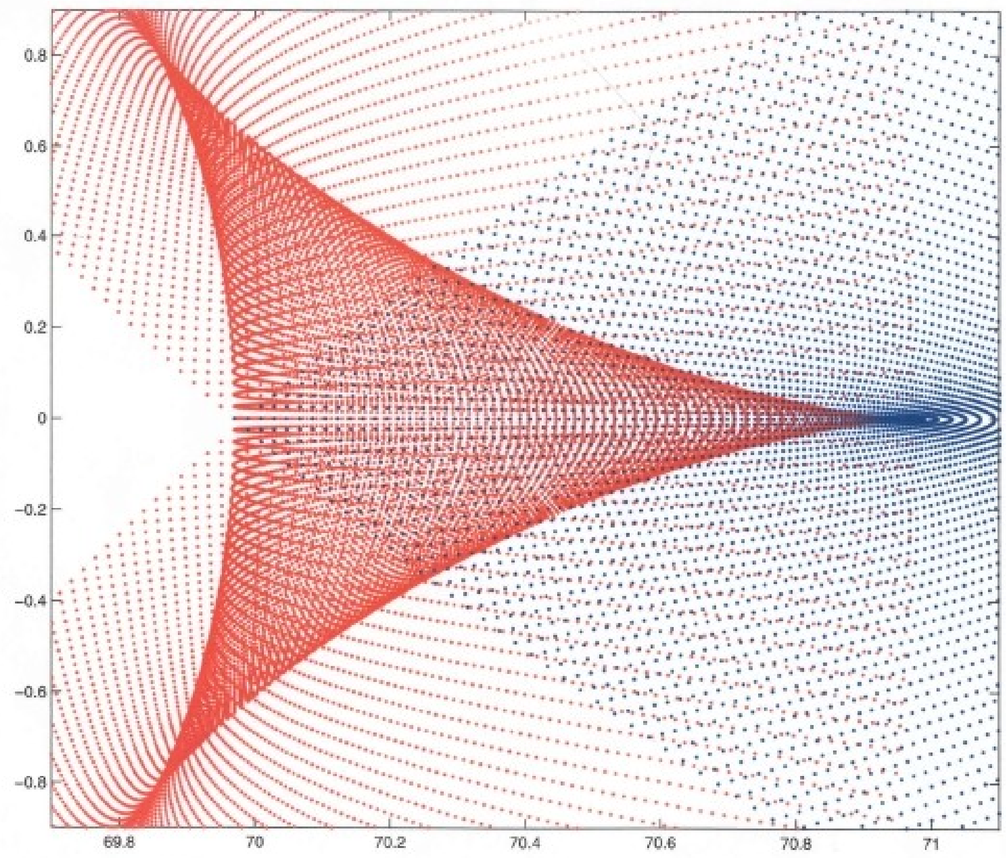

D_{-4}

an elliptic umbilic catastrophe

The Big Flow

- density $$d_5 \approx 1.7\ 10^{-24}\ \mathrm{gr/cm^3}$$

  previous estimates of the total local halo density range from 0.5 to 0.75 10^{-24} gr/cm ^{3}

- velocity $$\vec{v}_5 \cong (470\,\hat{\phi} \pm 100\,\hat{r})\ \mathrm{km/s}$$

  $\hat{\phi}$ in the direction of galactic rotation

  $\hat{r}$ in the direction away from the galactic center

- velocity dispersion $$\delta v_5 < 50\ \mathrm{m/s}$$

Experimental implications

- for dark matter axion searches

 - peaks in the energy spectrum of microwave photons
   from $a \rightarrow \gamma$ conversion in the cavity detector

 - high resolution analysis of the signal yields a more
   sensitive search (with L. Duffy and ADMX collab.)

- for dark matter WIMP searches

 - plateaux in the recoil energy spectrum from elastic
   WIMP collisions with target nuclei

 - the flux is largest around December
   (Vergados; Green; Gelmini and Gondolo; Ling, Wick &PS)

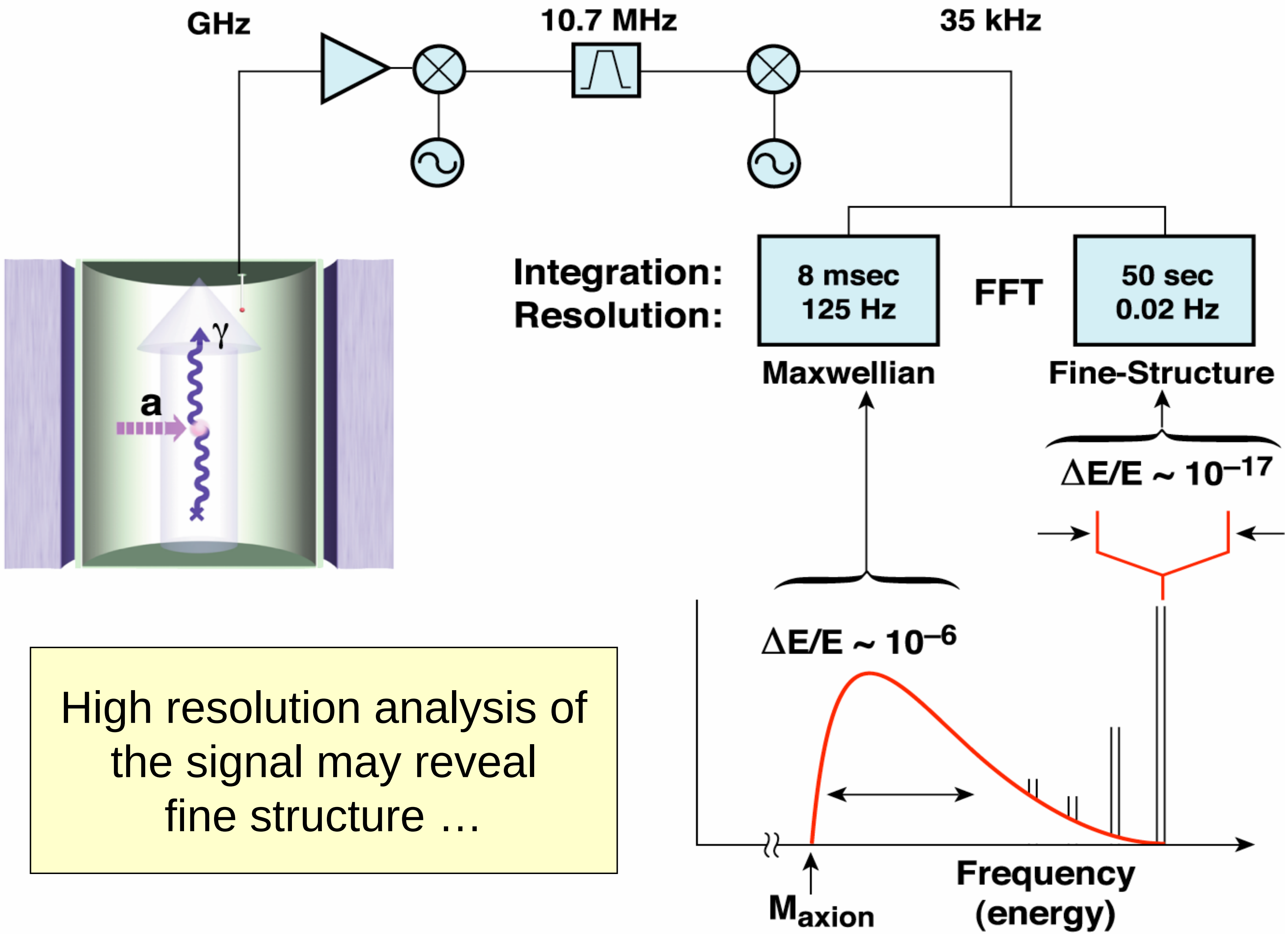

High resolution analysis of the signal may reveal fine structure …

an environmental peak, as seen

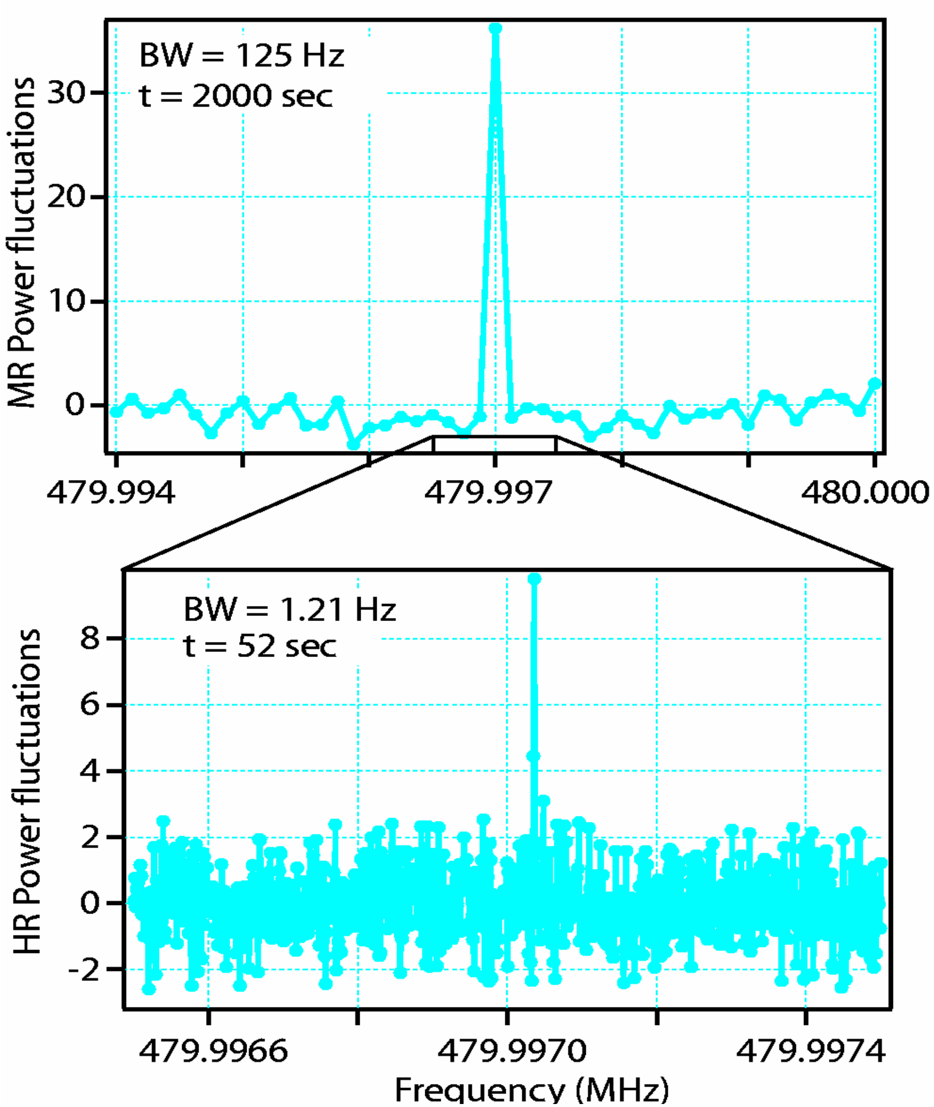

in the medium

and

high resolution channels

ADMX limit using high resolution (HR) channel

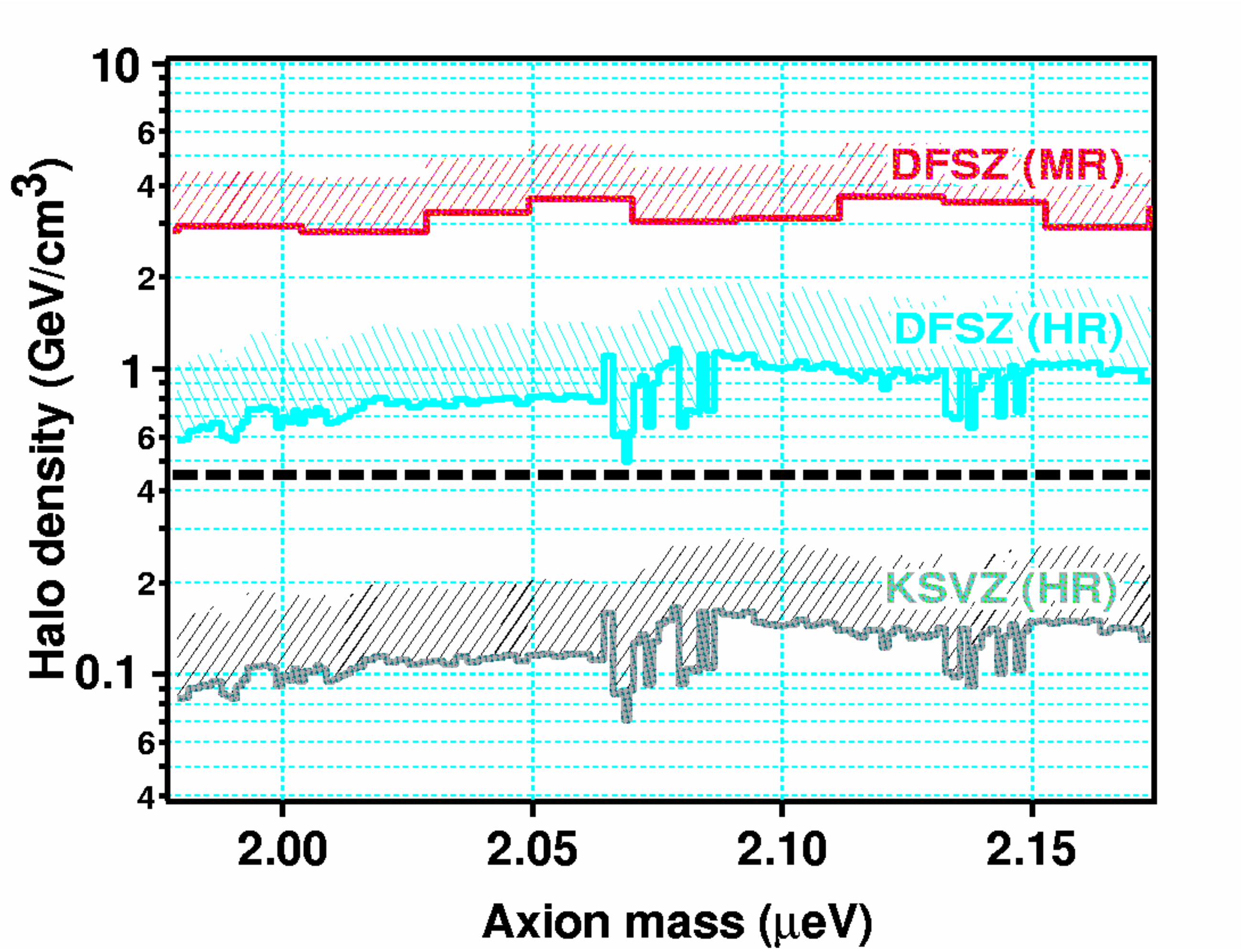

for $\delta v \leq 12\ m/s \left(\frac{300\ km/s}{v}\right)$

Axion to photon conversion in a magnetic field

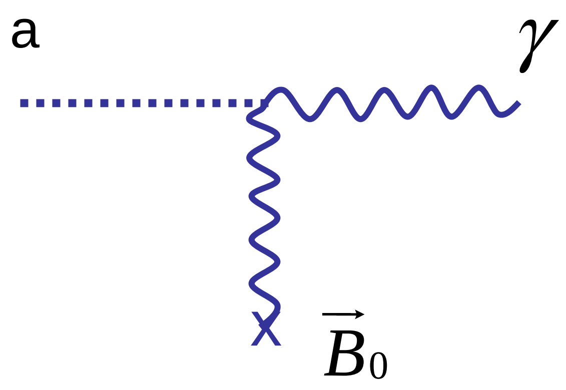

in vacuum probability

$$p(a \longleftrightarrow \gamma) = \left(\frac{\alpha\, g_\gamma}{\pi\, f_a}\right)^2 \mathrm{B}_0^{\,2} \left(\frac{\sin \frac{q_z L}{2}}{q_z}\right)^2$$

with $$q_z = \frac{m_a^{\,2} - \omega_{\mathrm{pl}}^{\,2}}{2E_a}$$

Theory

- P. S. '83
- L. Maiani, R. Petronzio and E. Zavattini '86
- K. van Bibber et al. '87
- G. Raffelt and L. Stodolsky, '88
- K. van Bibber et al. '89

Experiment

- D. Lazarus et al. '92
- R. Cameron et al. '93
- S. Moriyama et al. '98, Y. Inoue et al. '02
- K. Zioutas et al. 04
- E. Zavattini et al. 05

Cern Axion Solar Telescope

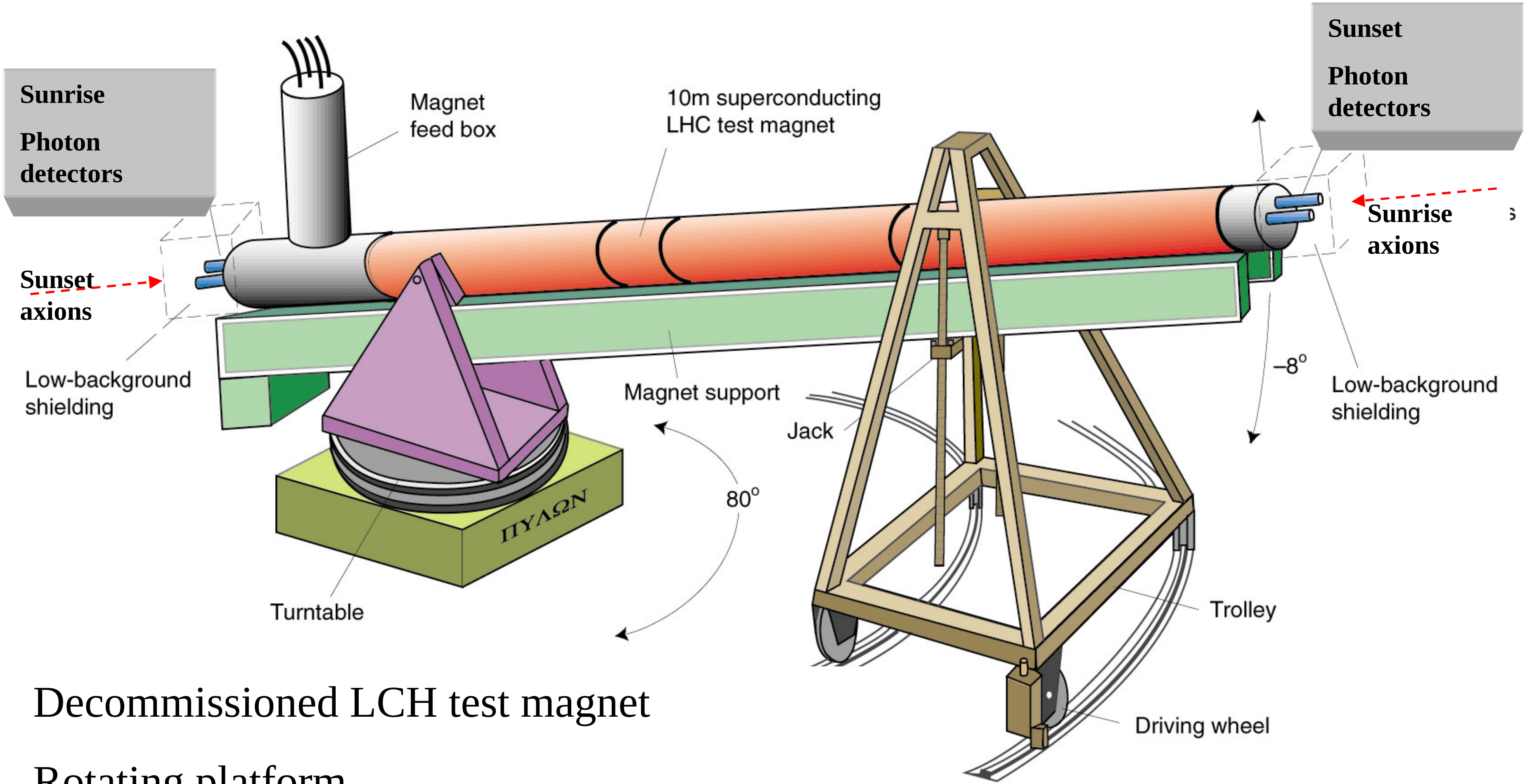

Decommissioned LCH test magnet

Rotating platform

3 X-ray detectors

X-ray Focusing Device


CAST
ANSALDO GIE
EUROPAMETALLI – LMI
E. ZANON

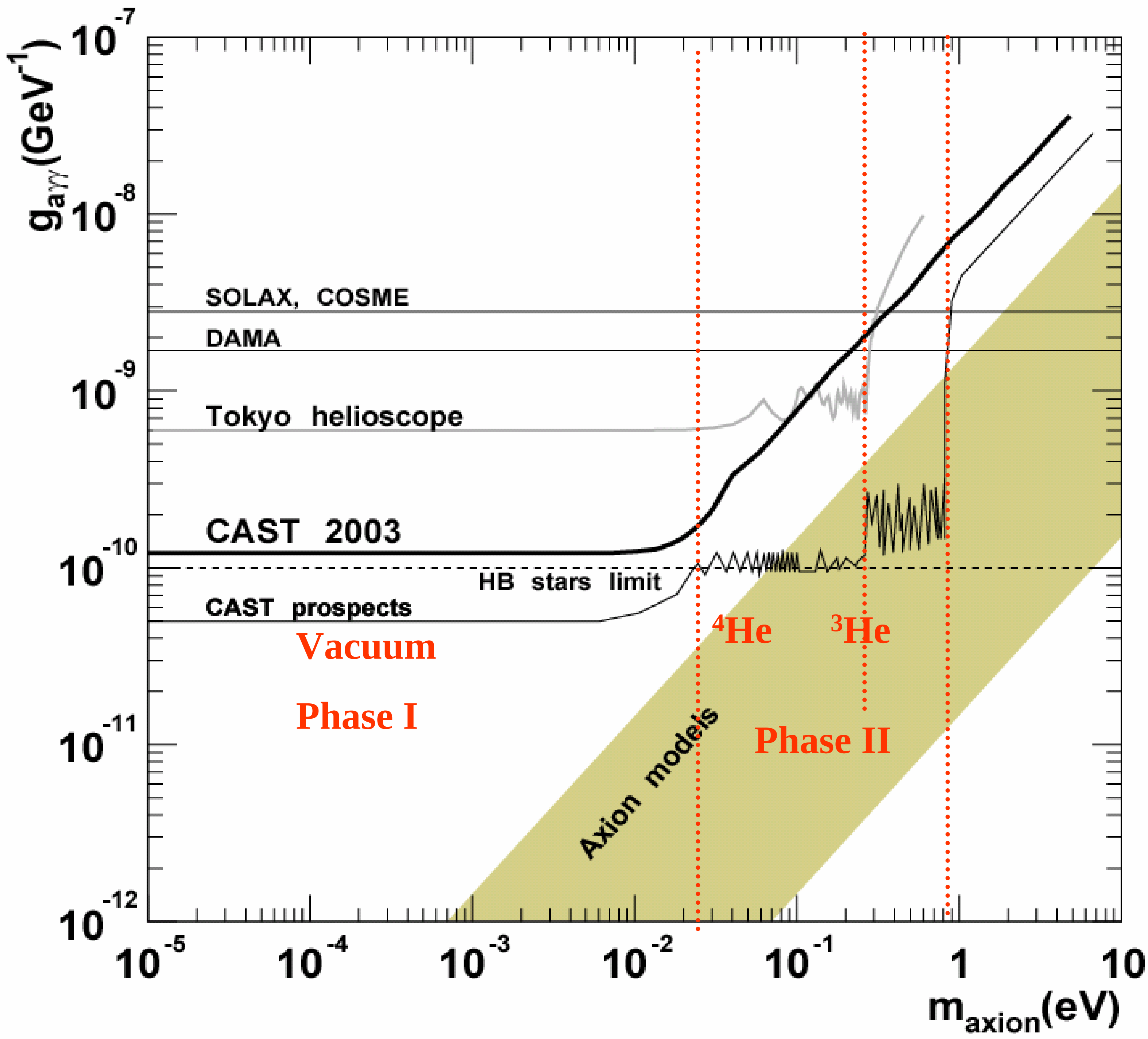

$g_{a\gamma\gamma}$ (GeV^{-1})
SOLAX, COSME
DAMA
Tokyo helioscope
CAST 2003
HB stars limit
CAST prospects
Vacuum
Phase I
^{4}He
^{3}He
Phase II
Axion models
m_{axion}(eV)

Detecting solar axions using Earth's magnetic field

by H. Davoudiasl and P. Huber

hep-ph/0509293

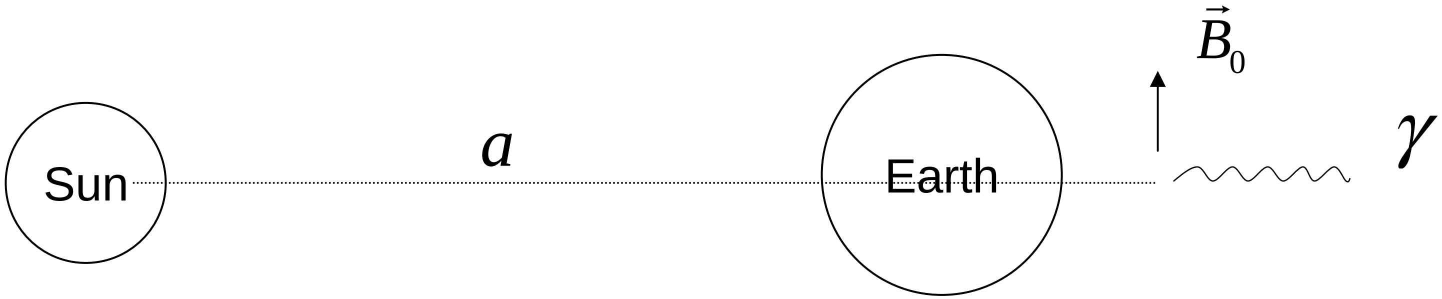

For axion masses $m_a \leq 10^{-4}\,\mathrm{eV}$, a low-Earth-orbit x-ray detector with an effective area of $10^4\,\mathrm{cm}^2$, pointed at the solar core, can probe down to $M_a \sim 10^{11}\,\mathrm{GeV}$, in one year.

$$(L_{a\gamma\gamma} = \frac{1}{M_a} a\, \vec{E} \cdot \vec{B})$$

Linearly polarized light in a constant magnetic field

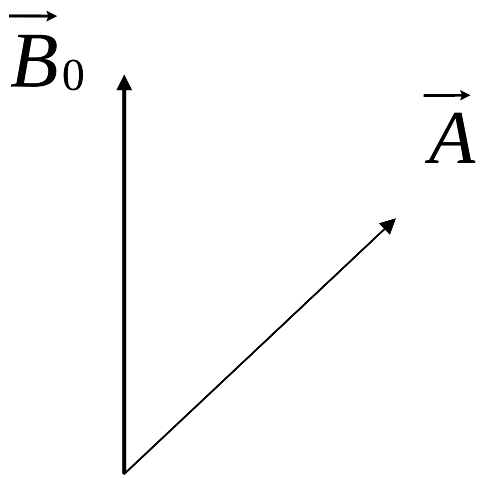

Rotation

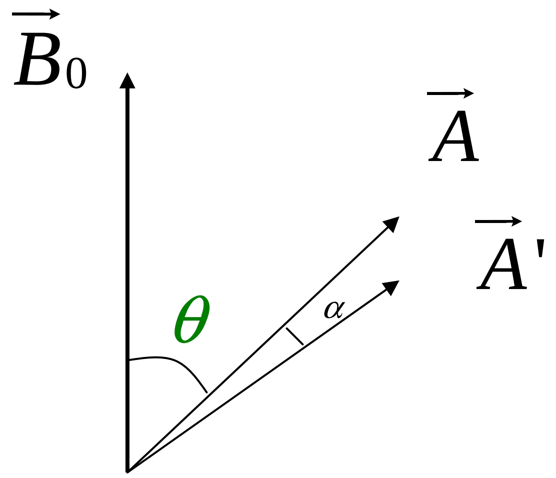

$$A'_{//} = A_{//}\,(1 - \frac{1}{2}p - i\psi)$$

$$A'_{\perp} = A_{\perp}$$

$$p = 4\frac{B_0{}^2\omega^2}{M_a{}^2 m_a{}^4}\sin^2\left(\frac{m_a{}^2 L}{4\omega}\right)$$

$$\frac{\alpha g_\gamma}{\pi f_a} = g_{a\gamma\gamma} = \frac{1}{M_a}$$

$$\alpha = -\frac{1}{4}p\sin(2\theta)$$

Rotation and Ellipticity

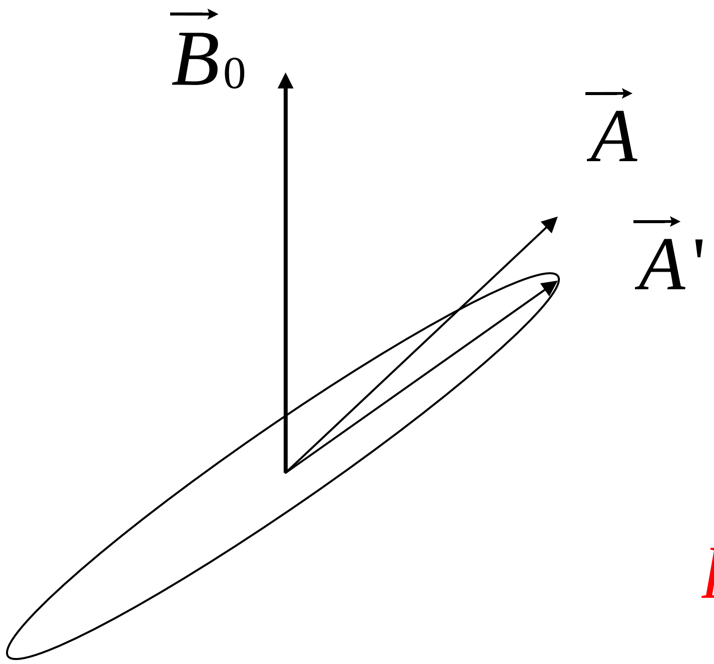

$$A'_{//} = A_{//}\left(1 - \frac{1}{2}p - i\psi\right)$$

$$A'_{\perp} = A_{\perp}$$

$$p = 4\frac{B_0{}^2\omega^2}{M_a{}^2 m_a{}^4}\sin^2\left(\frac{m_a{}^2 L}{4\omega}\right)$$

$$\frac{\alpha g_{\gamma}}{\pi f_a} = g_{a\gamma\gamma} = \frac{1}{M_a}$$

$$\psi = 2\frac{B_0{}^2\omega^2}{M_a{}^2 m_a{}^4}\left[\frac{m_a{}^2 L}{2\omega} - \sin\left(\frac{m_a{}^2 L}{2\omega}\right)\right]$$

Experimental observation of optical rotation generated in vacuum by a magnetic field

by E. Zavattini et al. (the PVLAS collaboration)
hep-ex/0507107

the average measured optical rotation is

$$(3.9 \pm 0.5)\ 10^{-12} \quad \text{rad/pass}$$

through a 5 T, 1 m long magnet

PVLAS

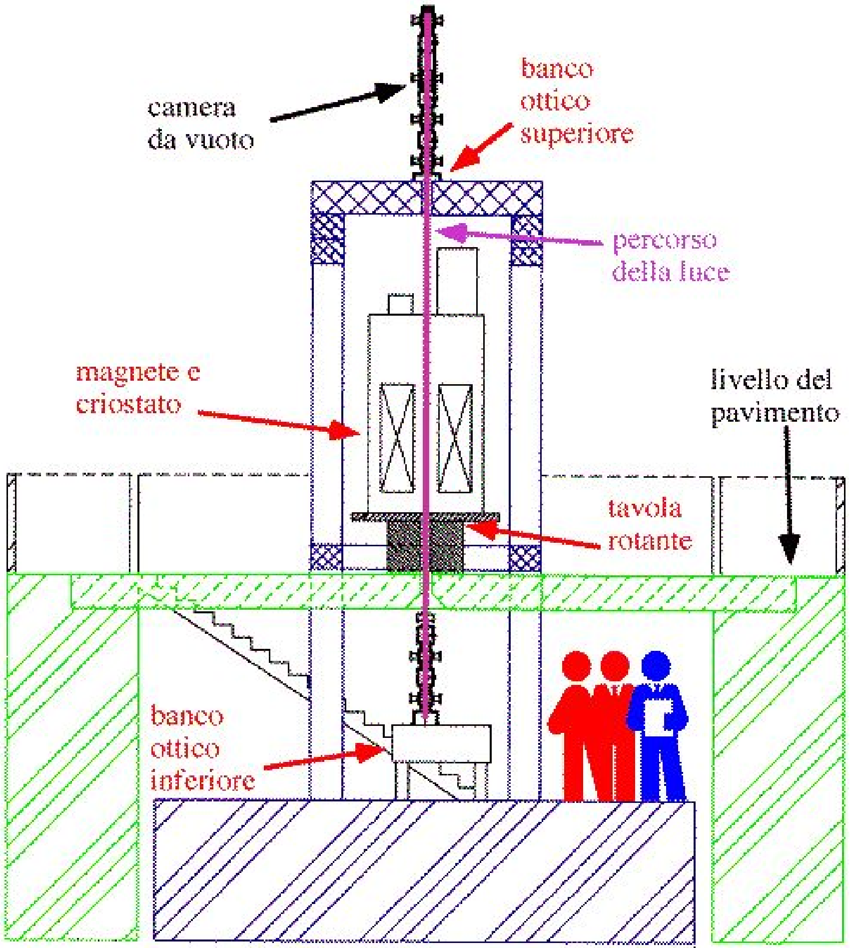
camera
da vuoto
banco
ottico
superiore
percorso
della luce
magnete e
criostato
livello del
pavimento
tavola
rotante
banco
ottico
inferiore

The PVLAS result can be interpreted in terms of an axion-like particle b

$$L_{b\gamma\gamma} = \frac{1}{M_b} b \, \vec{E} \cdot \vec{B}$$

$$1 \cdot 10^5 \text{ GeV} \leq M_b \leq 6 \cdot 10^6 \text{ GeV}$$

$$0.7 \, \text{meV} \leq m_b \leq 2 \, \text{meV}$$

inconsistent with solar axion searches, stellar evolution

descrepancy may be avoided in some models
E. Masso and J. Redondo, hep-ph/0504202

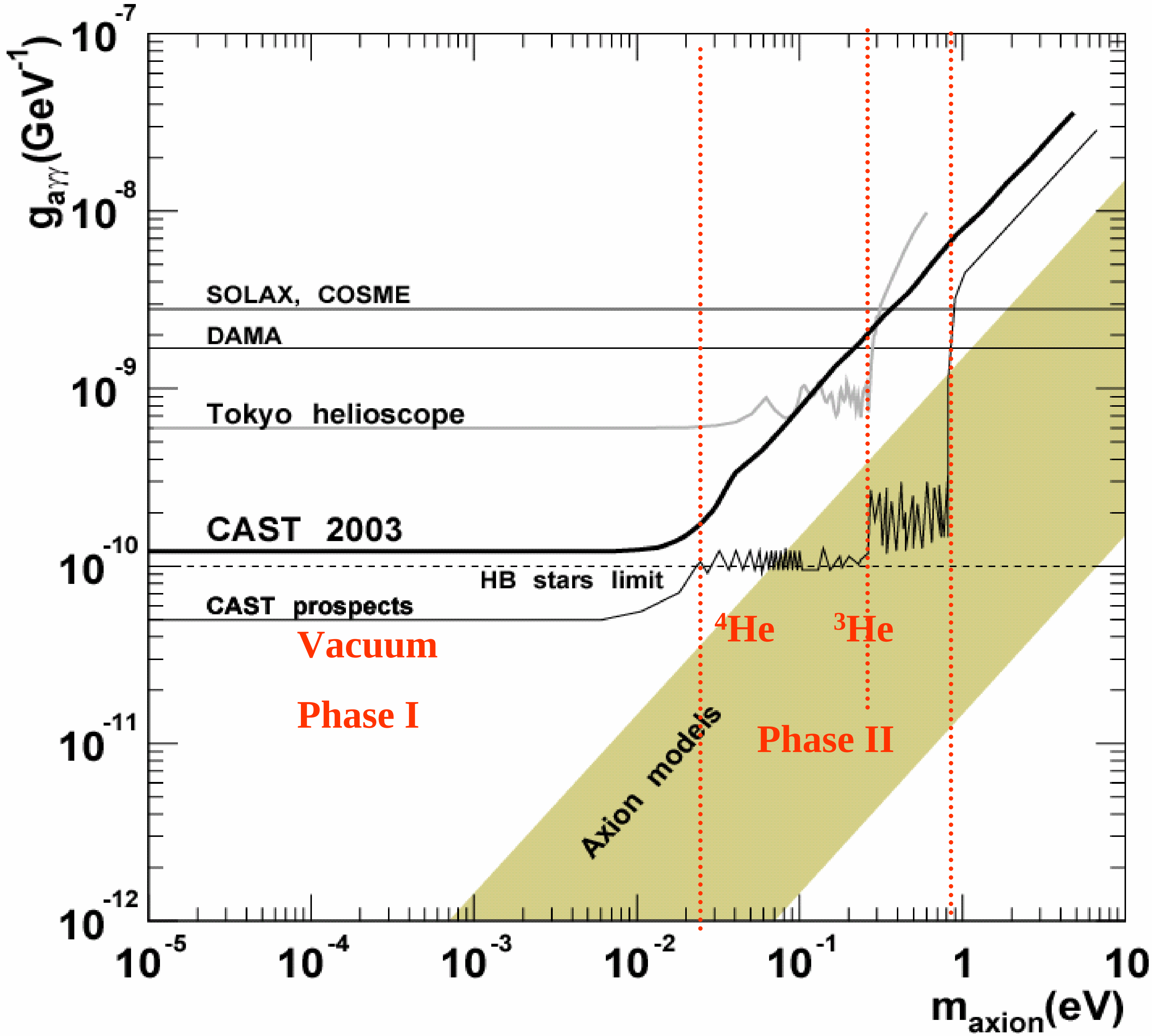

$g_{a\gamma\gamma}$ (GeV^{-1})
10^{-7}
10^{-8}
10^{-9}
10^{-10}
10^{-11}
10^{-12}
SOLAX, COSME
DAMA
Tokyo helioscope
CAST 2003
HB stars limit
CAST prospects
Vacuum
Phase I
^{4}He
^{3}He
Phase II
Axion models
10^{-5}
10^{-4}
10^{-3}
10^{-2}
10^{-1}
1
10
m_{axion}(eV)

Shining light through walls

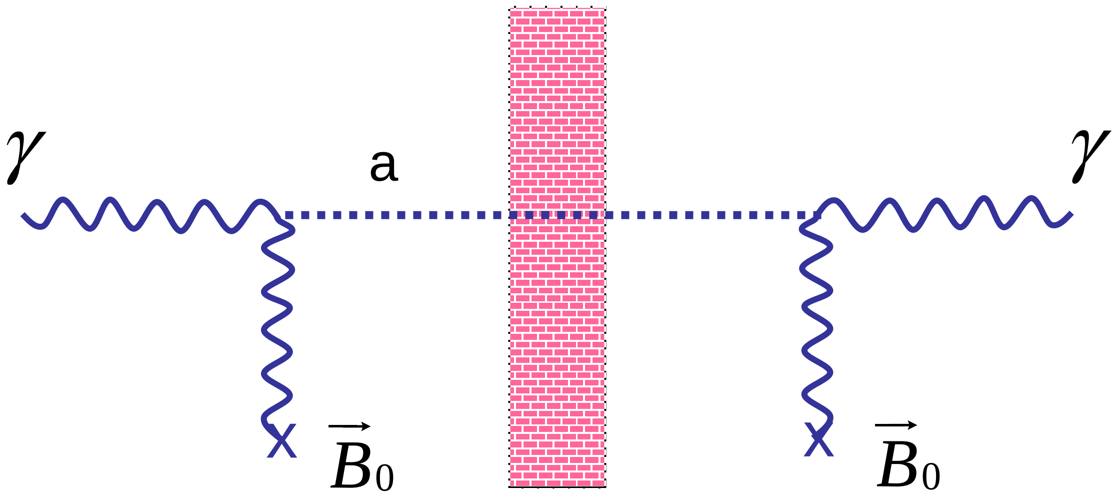

K. van Bibber et al. ‘87

A. Ringwald ‘03

P. Pugnat et al. ‘05

R. Rabadan, A. Ringwald and C. Sigurdson ‘05

$$\text{rate} \propto \frac{1}{f_a^{\,4}}$$

Primakoff conversion of solar axions in crystals on Earth

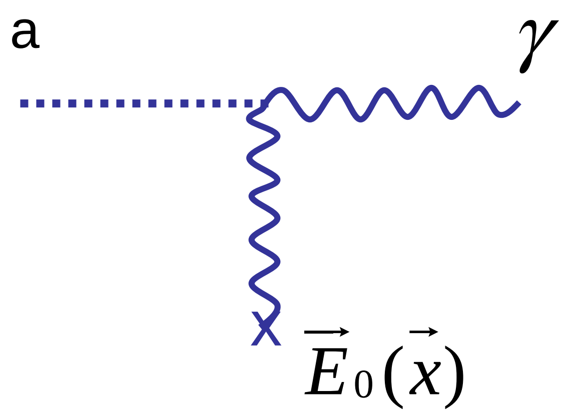

$E_a =$ few keV

Bragg scattering on crystal lattice

Solax, Cosme '98

Ge

DAMA '01

NaI (100 kg)

Ge

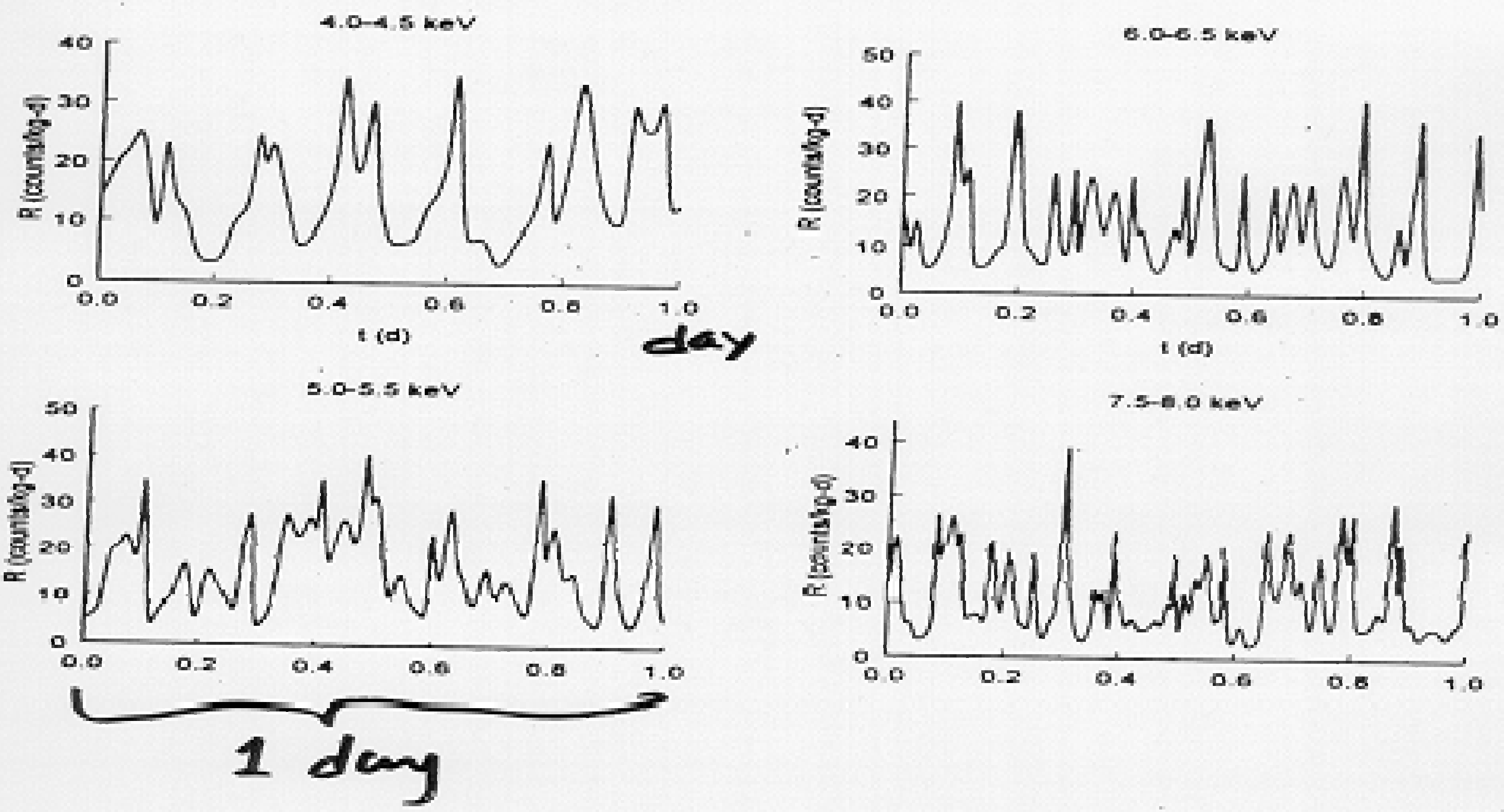

Changes every day

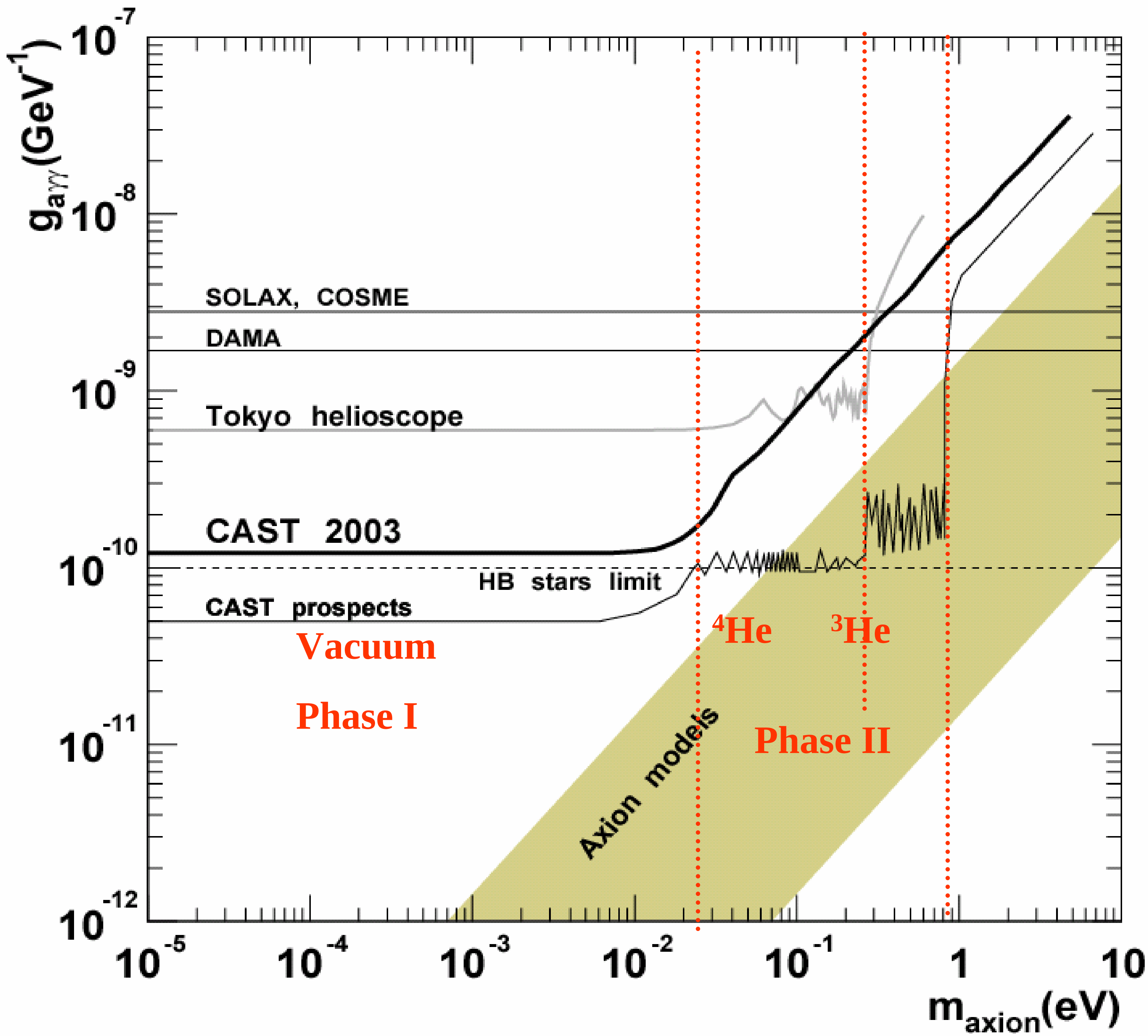

$g_{a\gamma\gamma}$ (GeV^{-1})
10^{-7}
10^{-8}
10^{-9}
10^{-10}
10^{-11}
10^{-12}
SOLAX, COSME
DAMA
Tokyo helioscope
CAST 2003
HB stars limit
CAST prospects
^{4}He
^{3}He
Vacuum
Phase I
Phase II
Axion models
10^{-5}
10^{-4}
10^{-3}
10^{-2}
10^{-1}
1
10
m_{axion}(eV)

Telescope search for cosmic axions

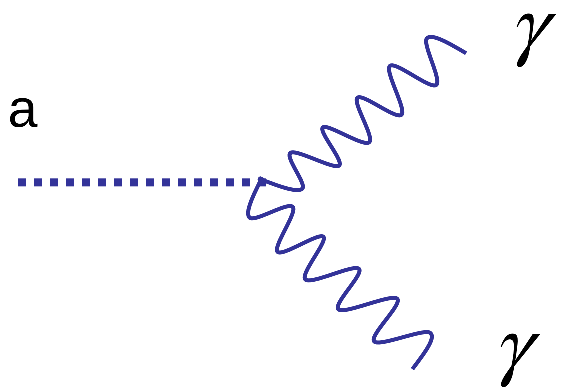

M.S. Bershady, M.T.Ressell and M.S. Turner '90

galaxy clusters

3 – 8 eV

B.D. Blout et al. '02

nearby dwarf galaxies

298 – 363 μeV

$g_{a\gamma\gamma} < 1.0 \cdot 10^{-9}$ GeV^{-1}

$$E_\gamma = \frac{m_a}{2}$$

$$\Gamma(a \to 2\gamma) = \frac{1}{0.67 \cdot 10^{25}\ \mathrm{sec}} \left(\frac{m_a}{\mathrm{eV}}\right)^5 \left(\frac{g_\gamma}{0.36}\right)^2$$

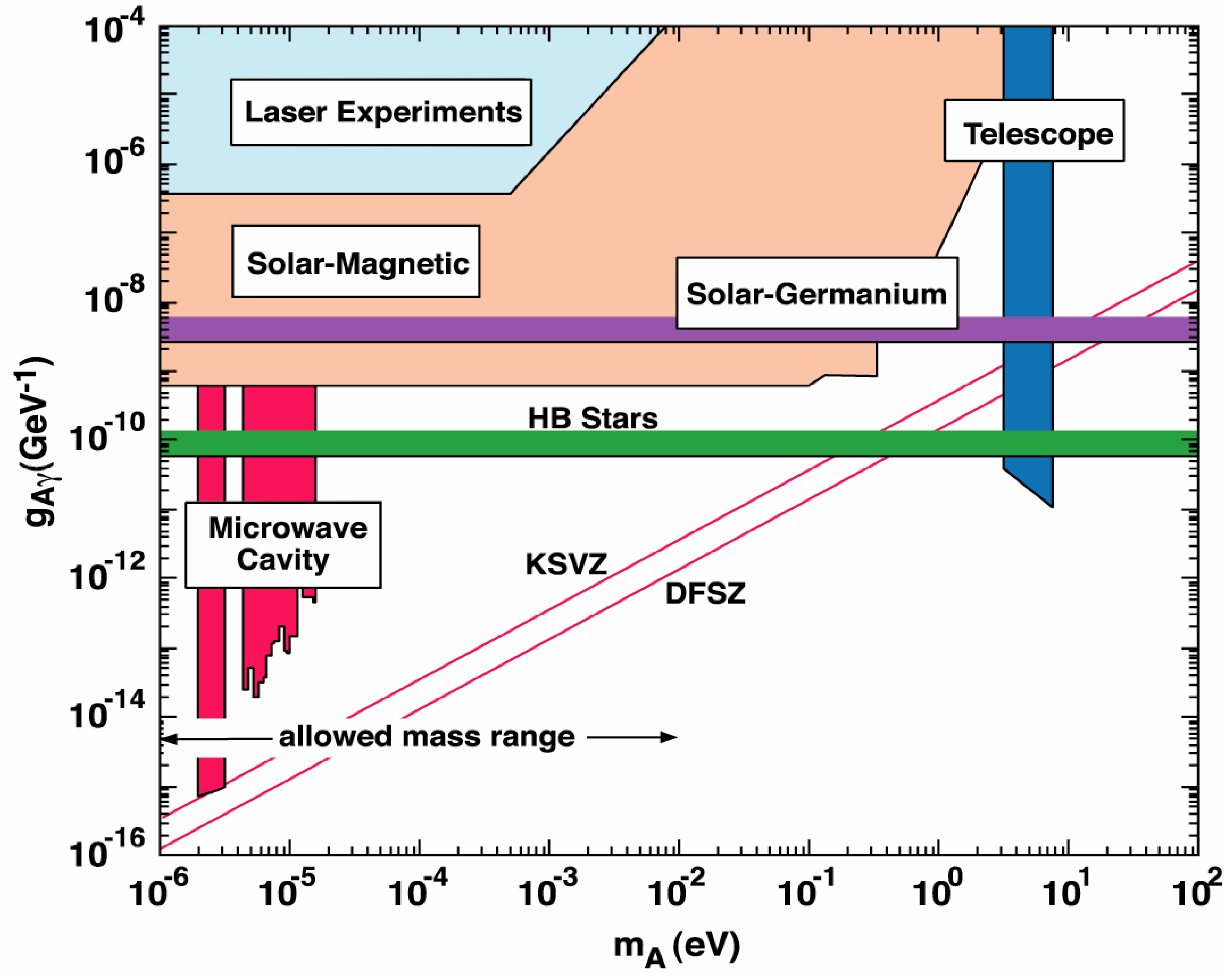

Laser Experiments
Solar-Magnetic
Solar-Germanium
Telescope
HB Stars
Microwave
Cavity
KSVZ
DFSZ
allowed mass range
10^{-4}
10^{-6}
10^{-8}
10^{-10}
10^{-12}
10^{-14}
10^{-16}
$g_{A\gamma}(GeV^{-1})$
10^{-6}
10^{-5}
10^{-4}
10^{-3}
10^{-2}
10^{-1}
10^{0}
10^{1}
10^{2}
m_A (eV)

Macroscopic forces mediated by axions

$$L_{a\bar{f}f} = g_f \frac{m_f}{f_a} a \bar{f} \left(i\gamma_5 + \theta_f \right) f$$

forces coupled to
the f spin density

background of
magnetic forces

forces coupled to
the f number density

$$\vartheta_f \lesssim 10^{-17}$$

Theory:

J. Moody and
F. Wilczek '84

Experiment:

A. Youdin et al. '96
W.-T. Ni et al. '96

Conclusions

Axions solve the strong CP problem and are a cold dark matter candidate.

If axions exist, they are present on Earth as dark matter and as particles emitted by the Sun.

If an axion signal is found, it will provide a rich trove of information on the structure of the Milky Way halo, and/or the Solar interior.

PVLAS

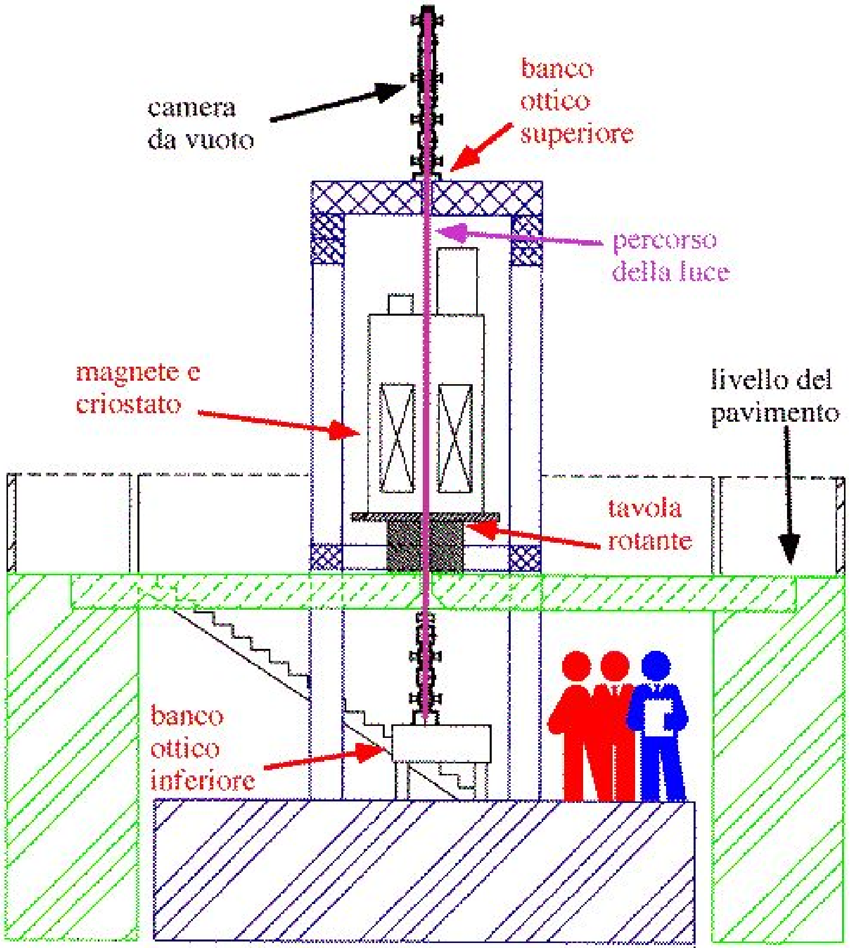
camera
da vuoto
banco
ottico
superiore
percorso
della luce
magnete e
criostato
livello del
pavimento
tavola
rotante
banco
ottico
inferiore

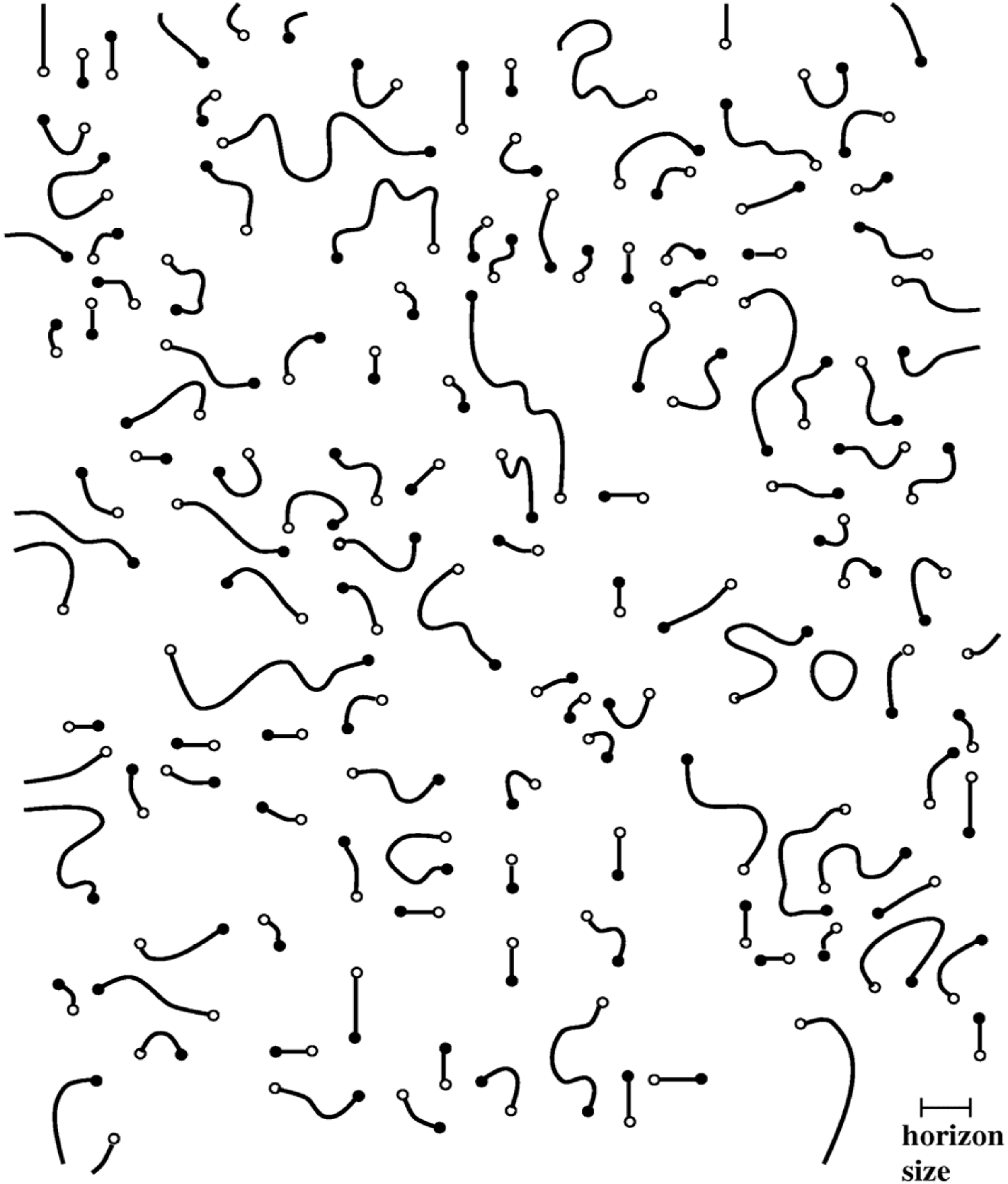

Axion
domain walls
bounded
by string
during the
QCD phase
transition

- the number of flows at our location in the Milky Way halo is of order 100
- small subhalos from hierarchical structure formation produce an effective velocity dispersion

$$\delta v_{eff} \leq 30 \text{ km/s}$$

  but do not destroy the sheet structure in phase space

- the known inhomogeneities in the distribution of matter are insufficient to diffuse the flows by gravitational scattering
- present N-body simulations do not have enough particles to resolve the flows and caustics

  (see however: Stiff and Widrow, Bertschinger and Shirokov)

Hierarchical clustering introduces effective velocity dispersion

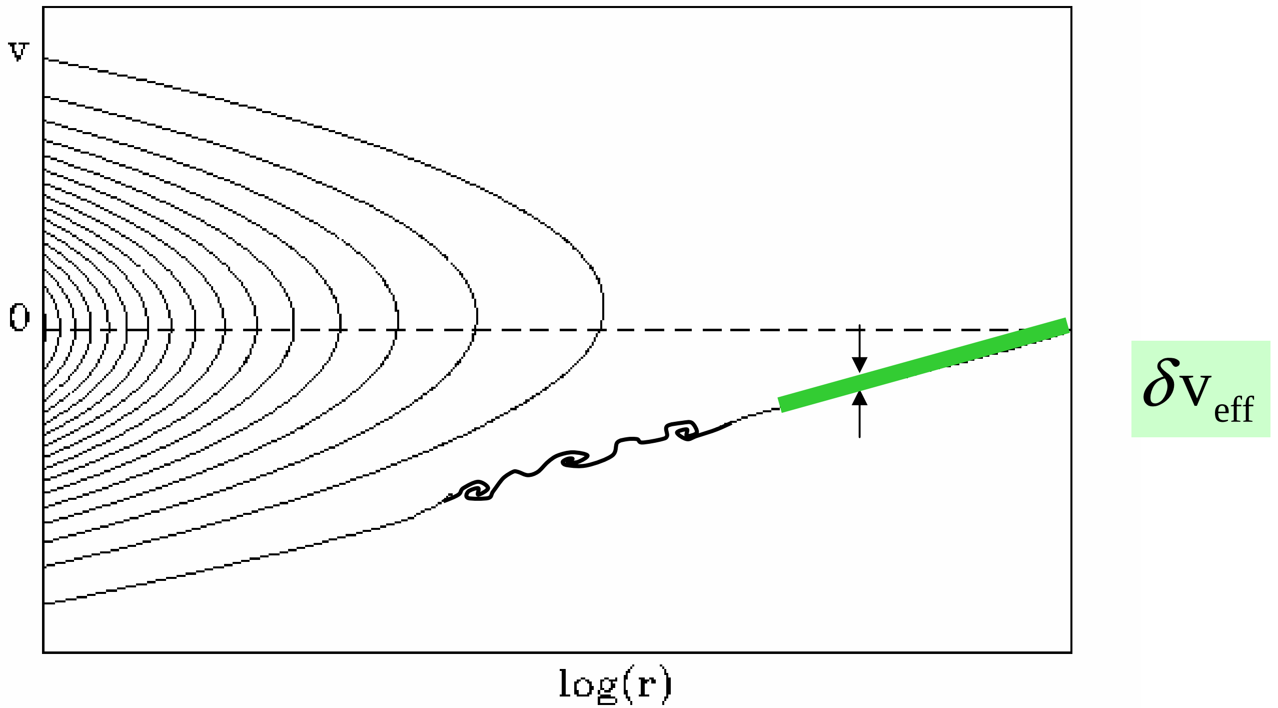

$$\delta v_{eff} \leq 30 \text{ km/s}$$

A shell of particles, part of a continuous flow.

The shell has net angular momentum.

As the shell falls in and out of the galaxy, it turns itself inside out.

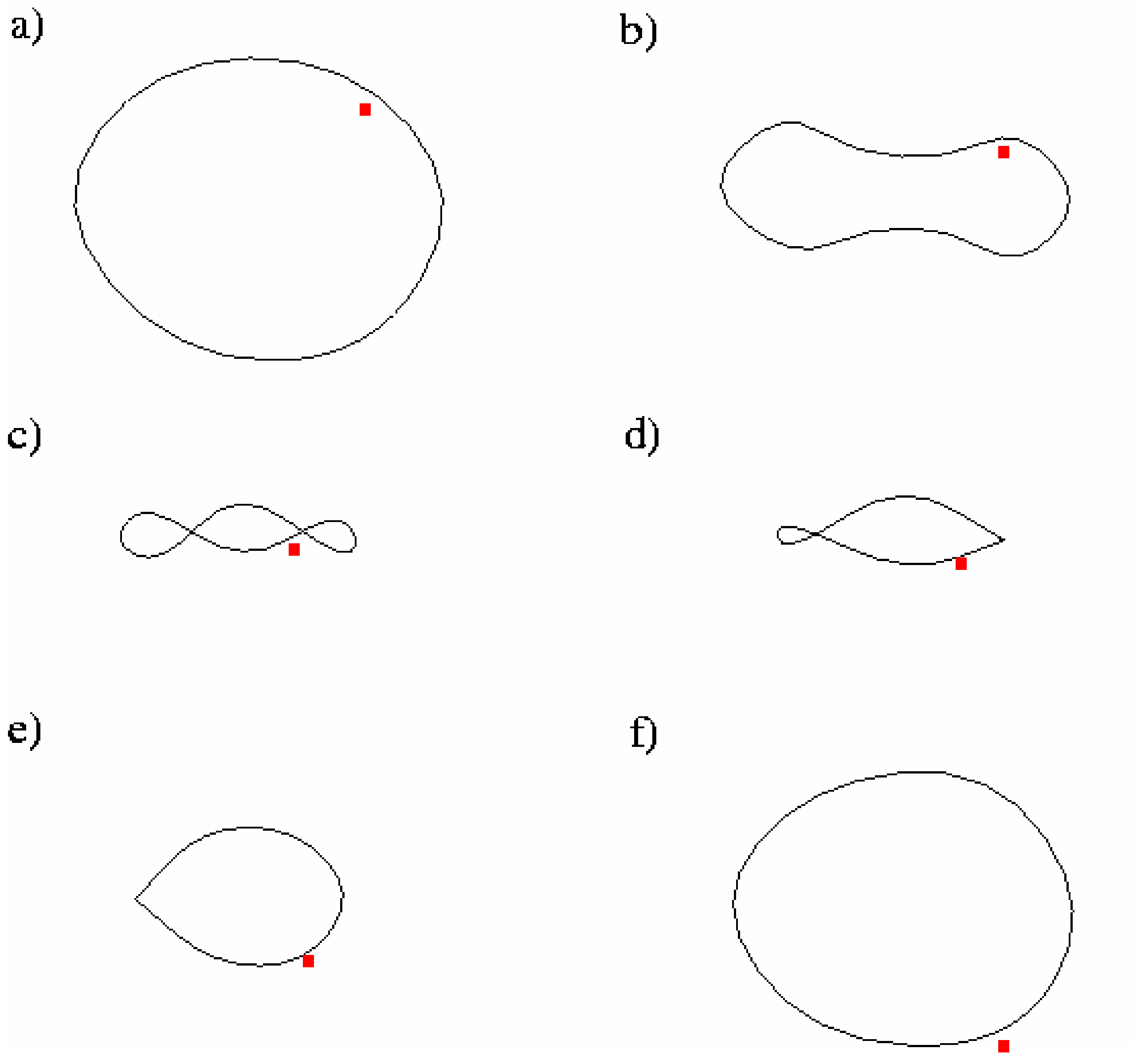

A caustic forms where the particles with the most angular momentum are at their closest approach to the galactic center.

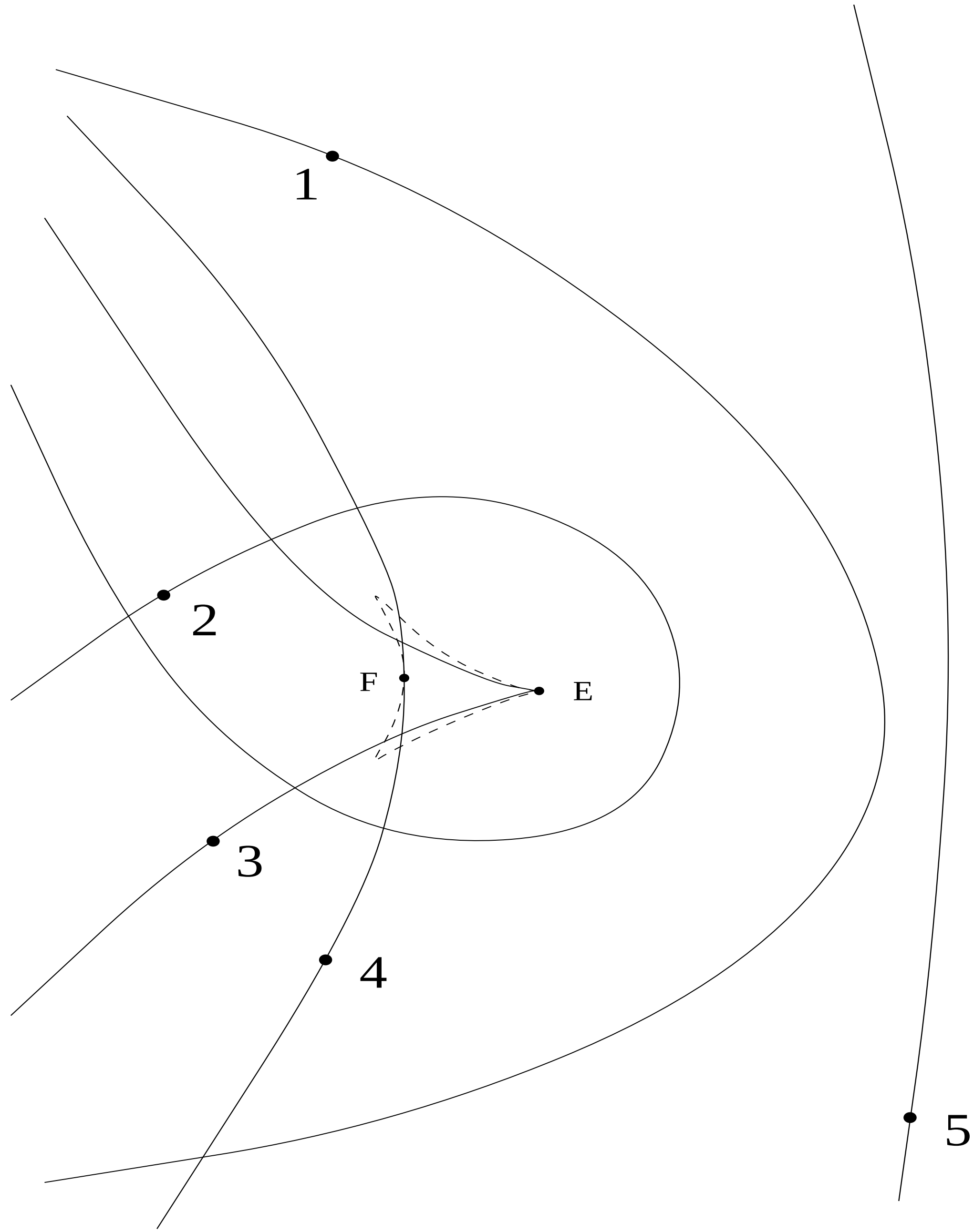

Spiral Arms vs. Caustic Rings of DM

- What causes the rises in the inner rotation curve of the Milky Way?
- Both spiral arms and caustic rings may contribute
- However, here are some reasons to believe that caustic rings of dark matter are the main cause:

  - the number of rises between 3 and 8.5 kpc is approximately 10, which is the expected number of caustic rings, whereas only 3 spiral arms are known in that range (Scutum, Sagittarius, and Local)

  - the rises are sharp transitions in the rotation curve, both where they start and where they end. The sharpness of the rises is consistent with the fact that the dark matter density diverges on caustic surfaces

  - bumps and rises are present in rotation curves at galactocentric distances much larger than the disk radius, where there are no spiral arms seen.

ADMX Upgrade: replace HEMTs (2 K) with SQUIDs (50 mK)

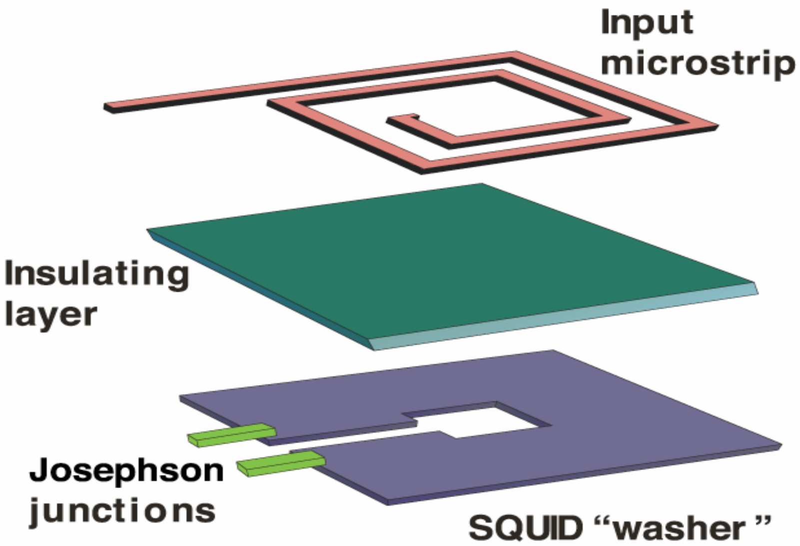

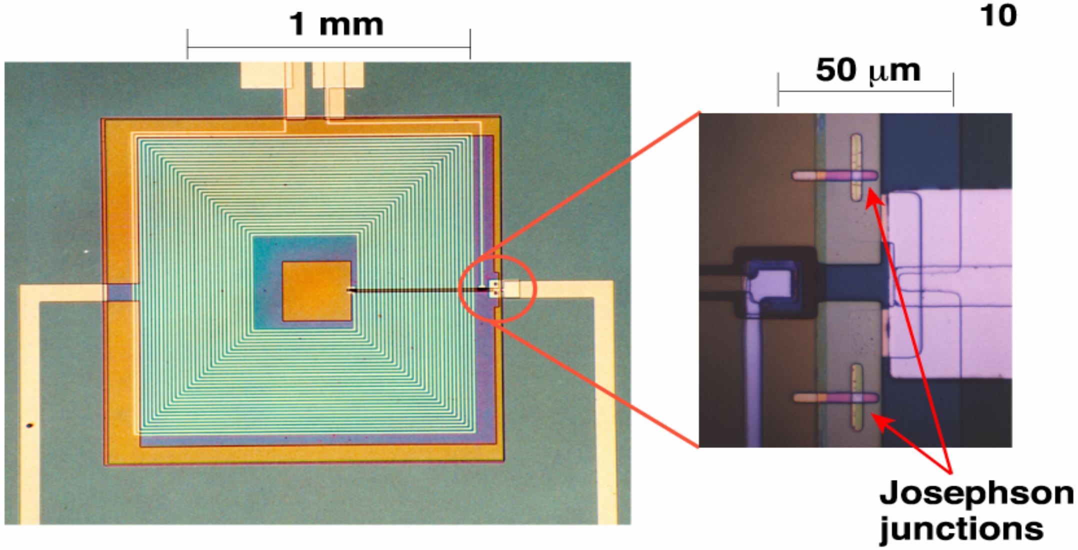

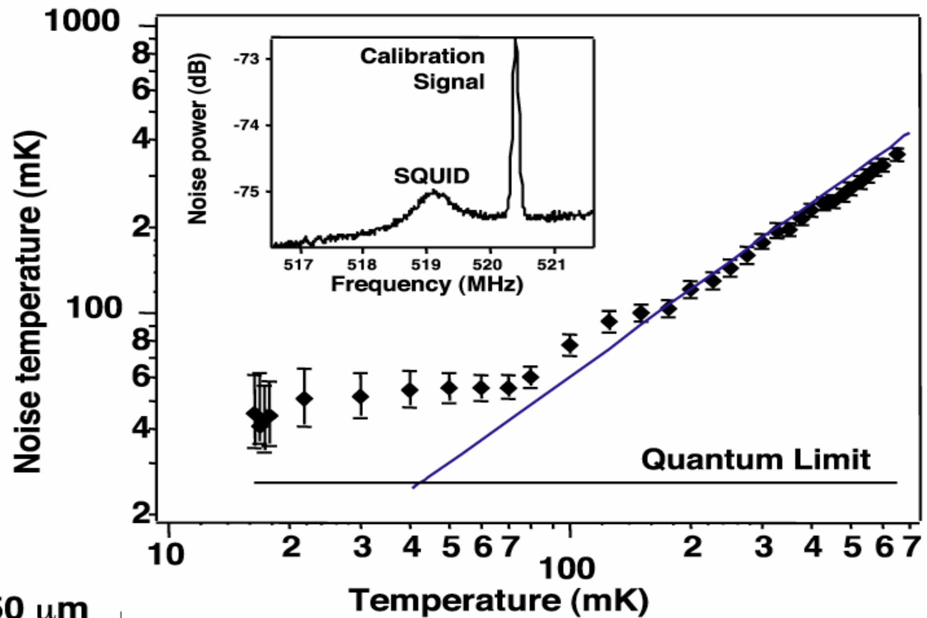

(J. Clarke *et al.*, U.C. Berkeley)

In phase II of the upgrade, the experiment is cooled with a dilution refrigerator.